Determination of Groundwater Storage Variation, Deficit, and Abstraction in Afghanistan and the Assessment of the Evolution of Vadose Zone in Kabul City

Mohammad Taqi Daqiq, Ravi Sharma, *Member, IEEE*, Anuradha Karunakalage, and Suresh Kannaujiya

***Abstract*— Groundwater is Afghanistan's main water supply resource, but the insufficient information and mismanagement of the surface and groundwater system have resulted in an alarming shortage of this precious resource. The monthly groundwater storage variation (ΔGWS) has been calculated in millimeter (mm) with a trend (mm/month) for the time interval of April 2002–October 2021 using the Gravity Recovery and Climate Experiment (GRACE) dataset for five major river basins of Afghanistan. A maximum and a minimum deseasonalized ΔGWS are observed at Amu Darya (246 to −253 mm) and Hari Rud (89 to −102 mm) basins, respectively. Subsequently, the GWS deficit (GWSD) and GWSD index (GWSDI) were calculated, and a negative GWSDI value signified the groundwater drought. Analysis of the GWS abstraction (GWS_{abs}) has also been carried out for the entire country. The estimated GWS_{abs} trend gives a maximum value of 12.60 mm/year in the northeast and southwest parts of the country. A spatiotemporal analysis showed the maximum GWS_{abs} variation up to 23.12 mm in 2021. Two phases of land deformation were determined in Kabul City using the interferometric synthetic aperture radar (InSAR) technique. In phase-I (2015–2017), there is a gentle negative trend [−20.66 mm/year in Upper Kabul (UKBL) and −18.54 mm/year in Lower Kabul (LKBL)], but in phase-II (2018–2020), there is a high negative trend (−151.34 mm/year in UKBL and −145.32 mm/year in LKBL). Overall, the entire country is experiencing a severe groundwater decline, apparently from the interplay of hydroclimatic and anthropogenic factors, which are most dominant in the Southern and Western parts of Afghanistan.**

***Index Terms*— Gravity Recovery and Climate Experiment (GRACE), groundwater storage abstraction (GWS_{abs}), GWS deficit (GWSD), GWS variation (ΔGWS), interferometric synthetic aperture radar (InSAR), land deformation.**

I. Introduction

GROUNDWATER is the world's leading freshwater resource for agriculture, industry, public supply, and ecosystems [1], [2]. It is the third largest water store after the ocean and the cryosphere. However, some areas utilize more groundwater than is replenished, resulting in the depletion of groundwater storage (GWS) [3]. GWS depletion has occurred in numerous parts of the world during the last several decades, including north China [4], northwest India [5], [6], [7], and the California Central Valley, USA [8]. Globally, GWS depletion might only be considered significant for the sea level rise (mostly apparent), when viewed in completeness with the location of the terrain (usually the coastal region), the seawater intrusion, and the resulting interaction between the changing fluid and the local rock causing zones of weakness and final subsidence.

Research and reports show that the severe groundwater shortage in Afghanistan over the last two decades resulted from global and regional droughts and overexploitation for irrigation purposes. Deep-drilled wells have been a more prevalent source of irrigation water in recent years in the Kabul and Helmand rivers basins. In the absence of actively operating competent authority for regulating or analyzing the groundwater situation, it is evident that the future of sustainable groundwater usage in Afghanistan will be bleak. The depletion and pollution of groundwater pose significant challenges when it comes to restricting its use for drinking water provision. This issue is of utmost concern in water management principles and strategies due to the paramount importance of ensuring access to safe drinking water for the population.

Due to the dry environment and limited surface water resources in Afghanistan, adequate water supply can only be obtained by digging wells into aquifers to acquire groundwater [9]. Historically, the local people relied on Karez systems to transport water, which uses unconfined aquifers in alluvial fans recharged by snowfall throughout the spring. The Karez system, which dates back 3000 years, is a classic subhorizontal tunnel that uses gravity to bring underground water to the surface [10], [11].

Currently, groundwater is extracted sporadically throughout Afghanistan using diesel motors, electrical submersibles, and solar pumps, mainly for irrigation purposes, with unrestricted extraction by nongovernmental organizations (NGOs), farmers, opium planters, warlords, and the corporate sector [12]. Recent studies have represented dramatic water stress in Kabul and the country with short-term droughts [12], [13], [14].

Manuscript received 8 December 2022; revised 14 June 2023 and 22 July 2023; accepted 19 September 2023. Date of publication 20 October 2023; date of current version 3 November 2023. *(Corresponding author: Ravi Sharma.)*

Mohammad Taqi Daqiq, Ravi Sharma, and Anuradha Karunakalage are with the Indian Institute of Technology Roorkee, Roorkee, Uttarakhand 247667, India (e-mail: mohammad_td@es.iitr.ac.in; ravi.sharma@es.iitr.ac.in; anuradha_s@es.iitr.ac.in).

Suresh Kannaujiya is with the Indian Institute of Remote Sensing, Indian Space Research Organization, Dehradun, Uttarakhand 248001, India (e-mail: skannaujiya@iirs.gov.in).

Digital Object Identifier 10.1109/TGRS.2023.3326164

Minimal studies on Afghanistan related to terrestrial water storage (TWS) and water resource availability have been conducted.

Some research on climate change shows that meteorological droughts are the major causes of water stress [15]. So far, no research has been done specifically on the variations of groundwater resources using the Gravity Recovery and Climate Experiment (GRACE) data in Afghanistan to cover the entire country. There is GRACE-based research on spatiotemporal TWS availability, sustainability, and reliability in Afghanistan by Sediqi et al. [16] that indicates a trend between (−0.43 and 0.00 cm/year) in the southwest region (Helmand basin) and more sustainability in the eastern part of the country. However, according to [16], climate change has caused changes in water availability in locations around Afghanistan, but anthropogenic factors are also considerably affecting GWS. Thus, it is the interplay of climate change and anthropogenic factors that could be attributed to the main reason for the tensive situation of groundwater in Afghanistan.

Overexploitation of groundwater, which alters the geodynamic state of the environment, can have negative environmental impacts, such as land subsidence and associated infrastructure damage [17], [18]. Groundwater abstraction can cause changes in hydraulic head, pore pressure, and effective stress, which can contribute to ground surface deformation [19], [20].

Kabul is the country's capital, with a population of more than five million population that has been ranked as the fifth fastest growing city in the world. Groundwater is the primary water supply resource for multipurpose of Kabul residences. There are four aquifer systems in Kabul for groundwater supply, including Upper Kabul (UKBL), Lower Kabul (LKBL), Paghman (PGHMN), and Logar aquifers. Recently, news has revealed land subsidence in Kabul, but only research has been done by Meldebekova et al. [21].

After the GRACE mass concentration blocks called mascon solutions introduced by the Jet Propulsion Laboratory (JPL) of National Aeronautics and Space Administration (NASA) and Center for Space Research (CSR), University of Texas, under the RL06 data product with high spatial resolution and different processing steps [22], [23], the RL-06 CSR-Mascon data product has not required postprocessing [24]. Throughout the last decade, the research based on GRACE TWS data has focused on the discussion of groundwater stress worldwide. Therefore, the present study quantifies GWS changes and groundwater deficit along with groundwater mass abstraction over the major river basins of Afghanistan using GRACE data. Simultaneously, we determined that groundwater overexploitation caused land deformation in Kabul using synthetic aperture radar (SAR) data between 2015 and 2020.

SAR is a microwave remote sensing technology in which microwave beams are delivered from the antenna to the Earth's surface. Backscattered energy is measured using the radar principle to create a picture. The amplitude of the reflected wave may be used to determine the target's surface composition and size. The two-way travel time is used to calculate the distance between the satellite and the ground surface. The narrower the beam and the higher the resolution in the direction of the flight track, the larger the antenna [25]. Large antennas, on the other hand, are not possible. As a result, the Doppler principle is used in SAR technology. By broadcasting and receiving radio waves during flight, SAR creates a virtual antenna with a large aperture size. The pulsewidth of a transmitting wave should be as small as feasible to increase range resolution. A small pulsewidth, on the other hand, has a more significant likelihood of being interfered with by noise.

The raw data for the SAR image are transformed into the single-look complex (SLC) format. SLC provides both phase and amplitude information in the form of complex numbers. Phase values describe the delay in the time of the received signal in a coherent system. In contrast, amplitude represents the fluctuation in brightness that indicates spatial variations in the physical features of the ground surface [26]. SLC is saved as a slant range that may be geocoded to the ground range.

The SAR satellite sees in an oblique downward orientation rather than immediately below. The satellite observes from the west side in ascending orbit (northward) and from the east side while in descending orbit (southward). If a satellite watches the ground moving west in ascending orbit (northward), the ground gets closer to the satellite. When a satellite observes from a lowering orbit (toward the south), the ground moves away from the satellite, which is called line-of-sight (LOS) displacement.

The estimations from GRACE/GRACE-Following (FO) can provide a "big picture" of the nation's GWS variation (ΔGWS) on a regional scale. It has the potential to provide essential information for governmental authorities, policymakers, water resource managers, and the public. Hence, the present study aims to estimate GWS variation, abstraction, and deficit over the five major river basins during the last two decades. The extensive groundwater pumping in the capital of country has resulted in an adverse water level decline causing the evolution of vadose zone. A part of this research focused on revealing the invisible risk of vadose zone development in the form of land surface deformation.

II. Study Area

Afghanistan is in the Southwest region of Central Asia, with geographical coordinates of 29°35' N–38°40' N latitude and 60°31' E–74°55' E longitude. Afghanistan is surrounded by Uzbekistan, Tajikistan, and Turkmenistan from the north; in the west by Iran; in the south and southeast by Pakistan; and in the northeast by China. Afghanistan has a total area of 652 000 km^2. The country's geography is strongly undulating, with mountains covering 75% of the land.

Afghanistan has a subtropical and continental climate, with hot and sunny summers and cold and wet winters. According to the Köppen–Geiger climate classification, the nation has five climatic zones: arid desert, arid steppe, moderate dry summer, cold and dry summer, and polar tundra. The country's yearly average rainfall is 200–400 mm [27]. However, the rainfall variances are significant and vary according to height and location. The lowest mean annual precipitation of around 30 mm is reported for the Southwest part of the country, while the highest precipitation is occurring in the Northeast Hindukush and Pamir mountains' foothill region around 1000 mm [28],

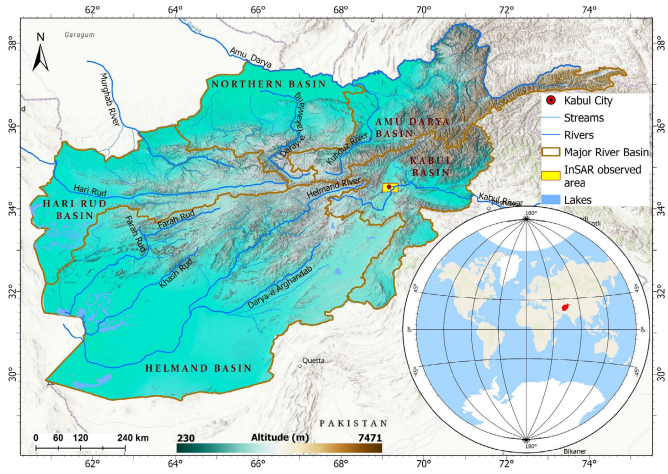

Fig. 1. Study area map shows the major rivers of Afghanistan with the blue line within respective river basins for GWS study. The InSAR observed area is determined with a yellow rectangle.

[29]. In contrast, the annual evapotranspiration reaches up to 1800 mm due to high temperature in the Southwest region and relatively low (1000–1300 mm) in the Hindukush region because of severe and long winter [30]. The South is arid, primarily desert-covered, and some parts of the Central and Northeast regions are frigid due to altitude. Even in the summer, East Asia is wet due to the partial impacts of the Indian monsoon. This region also has a wide variety of temperature changes. In January, the average temperature on the plains is between 0 °C and 8 °C, with absolute low temperatures ranging from 20 °C to 25 °C. In July, typical temperatures on the plains vary from 24 °C to 32 °C, with a 45 °C absolute maximum temperature [28]. Five major river basins drain Afghanistan: Kabul River basin, Amu Darya River basin, Northern River basin, Hari Rud River basin, and Helmand River basin (see Fig. 1). The GRACE data analysis is carried out grid-based over the country, but due to hydroclimatic variation of river basins in Afghanistan, we calculated the final results basin wise. Moreover, Afghanistan has basinal water management sections, so we wanted to stay focused on the basinal average values to target the community there. In this study, we generated all the GRACE-related maps using the kernel interpolation with barriers. This interpolation method interpolates over the recommended study area, including contamination zones of lakes and other surface water bodies; therefore, the kernel interpolation method is more accurate than other considerable methods that do not allow adjusting the barriers [31].

The Kabul River basin drains by the Kabul River, which flows to the Indus River in Pakistan. This basin is in the Eastern part of the country with a catchment area of 72 686 km^2. Amu Darya basin is located in the Northeast of the country with an area of 96 599 km^2. The Kunduz and Kukcha rivers drain this basin through the Amu River, which flows to the Aural Sea. The Northern basin is located in the North of the country with a total catchment area of 70 914 km^2 and consists of several watersheds. The basin outflow is discharging to Turkmenistan through the Murghab, Kushk, and Gulran rivers, reaching the Amu River. However, other rivers only flow inside the country, i.e., Balkhab, Samangan, Sar-e Pul, and Sherin Tagab rivers. Hari Rud river basin is located in west of the country with a catchment area of 77 596 km^2. The Hari Rud and Farah Rud rivers drain the basin flowing through the border of Iran. Helmand river basin is located in the Southern part of the country with an area of 327 801 km^2 [32]. The Helmand River drains this basin, which discharges to the Hamoon-e Helmand on the border of Iran.

The current study included all the major river basins for the GRACE study and focused on Kabul for the SAR study.

A. Geological Setting of Study Area

Afghanistan is a junction of different crustal and oceanic blocks. According to [33], a collection of alien terranes fused to Eurasia's southern edge by a sequence of consecutive accretionary processes starting in the Paleozoic and extending to the present [34]. The current structure of the country was created by Mesozoic (Cimmeride) and Tertiary (Himalayan) orogenic events, which resulted in the mountainous core (massif) and recent sedimentary deposition in the surrounding areas. According to [35], several tectonic plate fragments (microplates) broke away from Gondwanaland's southern "supercontinent" during the late Permian. One of them, the Afghan microplate, collided with the Eurasian continental plate in the Mesozoic. This orogenic event known as the "Cimmeride" (sometimes known as the "Hercynian") began in the late Triassic and ended in the Jurassic/Early Cretaceous (200–150 million years ago). The Paropamisus-Band-e Turkestan mountains, to the south of Faryab, were formed during the Cimmeride orogeny [35].

The Indian plate separated from Gondwanaland about the Early Cretaceous. It collided with the Eurasian plate in the Paleogene (late Paleocene and early Eocene), resulting in further orogenesis, crustal thickening, and crustal movement (Himalayan orogenic episode). The rest of the Afghan microplate is called (the Afghan Block) as well has been pressed southwestward at rates more than 1 cm/year in south of the Hari Rud fault [36].

Large aquifers are also found in the associated alluvial-filled extensional basins, limited by normal faults (through transpression) situated at northwest-trending strike-slip systems as massive thrust-fault stepovers [37]. The right-lateral Sorobi fault and the left-lateral Chaman–Paghman fault system, which exist inside the transpressional plate boundary block, are bordered to the east and west by the exotic crustal Kabul block while confined to the north by the Herat–Panjshir fault. The most productive aquifers in Afghanistan are found in these extensional basins, which are depicted as structural grabens [37].

The Kabul basin was formed during the Late Paleocene due to plate movements (Tertiary). It is bordered by metamorphic rocks, which are mostly underlain. The Herat–Panjsher main fault in the west, the Sorobi fault in the east, and the Chaman fault system in the southeast intersect these rocks, which are part of the Kabul block. They are shattered along the fracture and shear lines and tightly folded—even imbricated in some

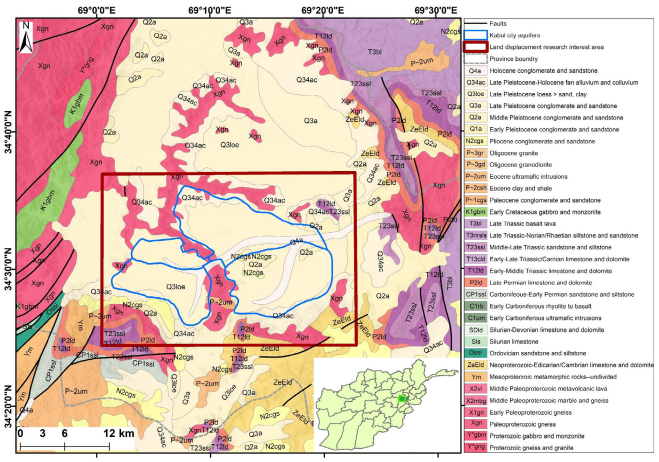

Fig. 2. Geological map of Kabul (inside the red box) and the surrounding area indicates the unconsolidated sediments in the aquifer system.

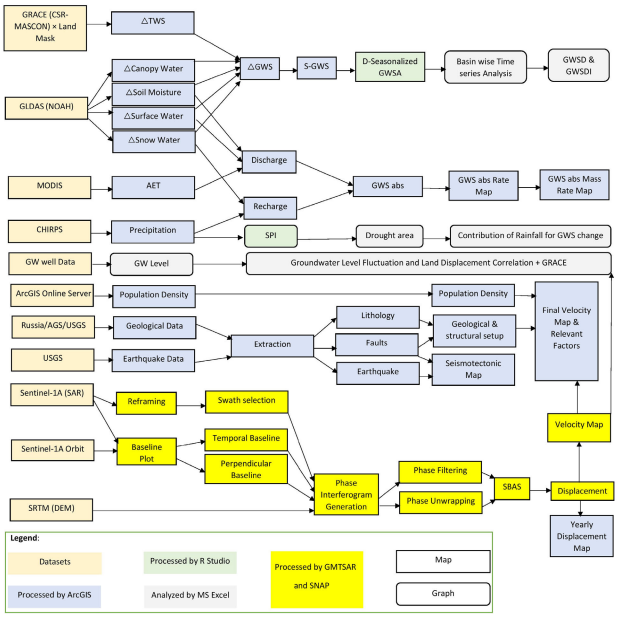

Fig. 3. Illustration of data processing and workflow.

places. Precambrian metamorphic basement (gneisses, granitic gneisses, amphibolite, mica schist, quartzite, and marbles) surrounds and underpins the Kabul basin, with some newer (upper Paleozoic–Mesozoic) limestone and marl on the south and east margins.

The basin is filled with consolidated and unconsolidated upper tertiary (Neogene) and quaternary clastic and alluvial deposits, mostly clay, sand, gravel, pebble, and conglomerate (see Fig. 2). The Kabul basin is filled with a mixture of terrestrial and lacustrine sediments, most of which are Neogene in age. Sand and gravel make up most of these deposits. Geophysical surveys found the overall thickness of the sediments to be up to 600 m [38].

III. Materials and Methods

The following spaceborne and ground-based datasets and different platforms have been used (see Tables I and II and Fig. 3). The exact address to access the data is provided under the section of data availability. The below datasets are used based on their availability, reliability, and accuracy. The following explanation justifies the use of the main datasets for this research.

GRACE (CSR-Mascon): This dataset is freely available. Moreover, based on the previous studies [5], [39], it has been shown that a high degree of correlation exists between CSR-Mascon and the other two free datasets, the JPL-Mascon and the Spherical Harmonic (SH), derived TWS change and GWS change with the rank correlation coefficient mostly > 0.9 [24]. In addition, among the GRACE solutions, the CSR-Mascon has the highest spatial resolution ($0.25° \times 0.25°$). Therefore, it was the obvious choice to stick with CSR-Mascon dataset to carry out the basinal scale analysis.

GLDAS Data (Hydrological Fluxes): Global Land Data Assimilation System (GLDAS) surface model dataset has been recommended in [3] as the most suitable auxiliary data of GRACE, which has the same spatial resolution as CSR-Mascon. Also, "GRACE-FO Level 3 user handbook" specifies using GLDAS surface model data for soil moisture (SM), surface water storage (SWS), plant canopy water (PC), and snow-melted equivalent water (SMEW) to estimate GWS from GRACE TWS data [40].

Sentinel-1A (SAR Data): Due to the minimal vegetation coverage of Kabul, the limitation of the penetration depth of the C-band pulse through the vegetation has not been considered. Therefore, Sentinel-1 (C-band) can effectively detect land subsidence in less vegetated area like Kabul [41].

A. GRACE-Derived GWS Change

This study conducted remote sensing and ground-based integrated observation to quantify the ΔGWS over the country and the resulting land deformation in Kabul. The monthly TWS is provided by NASA and processed at the CSR, University of Texas. CSR RL06 GRACE/GRACE-FO Mascon solutions version 02, level 3 with a spatial resolution of $0.25° \times 0.25°$ (25×25 km), is used for calculating the anomaly based on a time mean baseline from 2004 to 2009 covering all the months [3]. Due to repeated harsh weather conditions over multiple years, the GRACE solutions include seasonal and interseasonal cycles lasting more than one month. Furthermore, using an average monthly time mean baseline rather than a monthly variable baseline (interannual average as the average of each calendar month over multiple years) helps examine the climatology impact on ΔGWS over the research area for the considered time interval. The current study focuses on grid-wise ΔGWS rather than basin average to identify groundwater stress areas with human exploration and climate change as regulating factors. For determining monthly ΔGWS in each grid, the GRACE solution TWS anomaly (ΔTWS) is subtracted from the total monthly anomaly of all other effective hydrological fluxes using (1). The involved hydrological fluxes include SM, SWS, PC, and SMEW given by the GLDAS with 25×25 km spatial and monthly temporal resolution [42],

TABLE I
PRIMARY HYDROCLIMATIC AND DEMOGRAPHIC DATASETS HAVE BEEN USED FOR THE CURRENT STUDY

No	Dataset	Data Source	Data Model	Period	Spatial Resolution	Temporal Resolution
1	GRACE_CSR Mascon (TWS)	NASA Earth Data (GRACE Mission, GRACE-FO Mission)	CSR v2.0 RL06	2002-2021	25km× 25km	Monthly
2	SWS	Global Land Data Assimilation System (GLDAS)	NOAH v2.1 L4	2002-2021	25km × 25km	Monthly
3	SM					
4	SMEW					
5	PC					
6	Rainfall	Climate Hazards Group InfraRed Precipitation with Station (CHIRPS)	v 2.0	2002-2021	5km × 5km	Monthly
7	Actual Evapotranspiration (Central Asia)	Moderate Resolution Imaging Spectroradiometer (MODIS)	v 5	2003-2021	1km × 1km	Monthly
8	Kabul City Population Density	ArcGIS Online Server	N/A	2015	1km × 1km	N/A
9	Kabul Province groundwater level data	USGS and Afghanistan Geological Survey (AGS)	Standing Water Level (SWL)	2005-2012	N/A	Monthly
10	Kabul City groundwater level data	Ministry of Energy and Water (MEW), Afghanistan	SWL	2015-2019	N/A	Monthly

[43], [44]

$$\Delta \mathrm{GWS} = \Delta \mathrm{TWS} - (\Delta \mathrm{SMEW} + \Delta \mathrm{SWS} + \Delta \mathrm{PC} + \Delta \mathrm{SM}). \quad (1)$$

B. SPI and Seasonal GWS Anomalies

A time scale-independent probability of precipitation serves as the foundation for the standardized precipitation index (SPI). The observed precipitation probability is then converted into an index. More than 70 nations use it for operational or scientific purposes [45]. This study employed the SPI function in the standardized precipitation evapotranspiration index (SPEI) package with R studio to calculate the SPI values using (2).

The data collection of Climate Hazards Group Infrared Precipitation with Stations (CHIRPS) was used to compute pixel-based SPI values. The CHIRPS dataset was created using previous attempts at "Smart" interpolation methodologies, long-term rainfall records monitored with infrared cloud covering the duration, and rain gauge measurements with 0.05° × 0.05° spatial resolution and daily, pentad, and monthly temporal resolution [46].

TABLE II
SAR DATA FOR LAND DEFORMATION STUDY

No	1	2
Satellite Name	Sentinel-1A (European Space Agency)	Sentinel-1A (European Space Agency)
Data Source	Alaska Satellite Facility (ASF)	Alaska Satellite Facility (ASF)
Orbit	Descending	Ascending
Number of Scenes	28 (for processing in GMTSAR & SNAP)	2 (only for processing in SNAP)
Path	78	71
Target City	Kabul	Kabul
Period	2015-2020 Only for the dry season	2016-2020

The current study used 12-month SPI values to target GWS sensitivity with extreme weather conditions such as high-level rainfall in short periods and short-term (seasonal) droughts, both driven by climate change, and to understand the human influence on the groundwater system and hydro climatology breakdown consequences. The 12-month SPI is calculated by comparing the current month's precipitation to the same 12-month period in the historical data. For example, in previous records, the 12-month SPI number at the end of December corresponds to all total precipitation from January to December. Thus, 12-month SPI values more accurately reflect rainfall-related seasonal and interseasonal variations and extreme conditions [45]

$$^{t}_{\mathrm{grid}}\mathrm{SPI} = \frac{X - \overline{X_t}}{\sigma} \quad (2)$$

t is the probability distribution's time scale (12 months), $\overline{X_t}$ represents the mean value for the 12 months, and σ is the standardized deviation of the t month's probability distribution.

As a result, each drought event has a duration specified by its start and end dates and intensity for each month the event lasts. The "magnitude" of drought defines the positive total of the SPI for all months during a drought episode.

SPI values range from −2 to +2, and the drought category may be determined based on the SPI value of each pixel in each month. The nondeseasonalized (seasonal) ΔGWS time series has been reconciled with the SPI time series and series of drought area change to understand better the impact of seasonal and interseasonal droughts or wettest circumstances. The drought intensities based on the SPI using the categorization scheme presented in the SPI value (see Table III) have been classified in [47]. They also established the criteria for a drought occurrence across all periods. When the SPI is continually negative and reaches an intensity of −1.0 or

TABLE III
SPI CLASSIFICATION AND DROUGHT INTENSITY

2.00 +	Extremely wet
1.50 to 1.99	Very wet
1.00 to 1.49	Moderately wet
-0.99 to 0.99	Near Normal
-1.00 to -1.49	Moderately dry
-1.50 to -1.99	Severely dry
-2.00 and less	Extremely dry

less, it is considered a drought event. When the SPI reaches positive, the drought event is over.

C. GWS Anomalies Decomposition

The original ΔGWS time series derived from TWS includes a monthly related seasonal component. Due to irrigation intensities, land cover patterns and the location and morphology of river basins have a variety of weather patterns, particularly in terms of evapotranspiration and precipitation. As a result, the current research focuses on deconstructing grid-based seasonal patterns for each basin using the following equation [5]:

$$ {}^{t}_{\text{grid}}\Delta\text{GWS}_{\text{total}} = {}^{t}_{\text{grid}}\Delta\text{GWS}_{\text{long-term}} + {}^{t}_{\text{grid}}\Delta\text{GWS}_{\text{annual}} + {}^{t}_{\text{grid}}\Delta\text{GWS}_{\text{semi-annual}} + {}^{t}_{\text{grid}}\Delta\text{GWS}_{\text{residual}}. \tag{3} $$

The long-term trend component is combined with the long-term processes to form mid-to-long-term climatic oscillations that operate across the time series period. Temporal scaling and rapid system-related changes, such as aquifer nature, are required to deconstruct the long-term trend. Annual and semiannual phases make up the seasonal component. The annual changes in the groundwater system caused by recharge seasons are a cyclical process with a seasonal or recurring component. Groundwater dynamics, such as the seven-year El Nino impact, can also be cyclic overextended periods.

On the other hand, long-period cyclic processes are more likely to be detected by the trend component. Residuals or remainders are likely to indicate local mechanisms that produce variability across cycles and can thus be linked to short-term events or groundwater system consequences. These can be derived by subtracting the original signal's long-term trend and seasonal components.

We employed the seasonal trend decomposition using LOESS (SLT) for this investigation, as stated by Scanlon et al. [48]. The benefit of SLT decomposition is a flexible, robust approach that produces phase harmonics outputs comparable to the original after decomposition. The amplitude smoothing based on local regression (LOESS) is a critical process in SLT decomposition.

This study employed a 12-month moving time frame. According to earlier studies, a 12-month time range is an alternate way for detrending all small-scale disturbances, such as short-term trends and noises [49]. Identifying the long-term pattern of groundwater variability is the primary goal of eliminating the seasonal component. Groundwater has picked up long-term climatic oscillations as a measure for climatology changes due to the GWS-associated long-term climatic oscillations.

D. Sen's Slope and Mann Kendall Trend Statistic Calculation for Groundwater Trend Test

The Mann–Kendall test is a nonparametric test for detecting patterns in time series data. Rather than comparing the data values directly, the test evaluates the relative magnitudes of sample data [50]. One advantage of this test is that the data do not have to fit into any particular distribution. Furthermore, nondetect data include giving them a typical value less than the dataset's smallest measured value. The approach described in the following paragraphs assumes that each time series period has only one data value. The median value is utilized when there are many data points for a particular time interval. The Mann–Kendall statistic (S) compares each data value to the values after it. S has a zero value at the start (e.g., no trend). S increases by one if a data value from a later time series period is higher than a data value from an earlier time series period. Inversely, S decreases by one value if the data value is lower than the one collected earlier. The final value of S is the sum of all such increments and decrements. Considering $x_1, x_2, \ldots, x_n$ which, n is the number of data points where x_j is the data point at the time (j). Then, S is given [51] in below equation:

$$ S = \sum_{k=1}^{n-1} \sum_{j=k+1}^{n} \text{sign}(x_j - x_k) \tag{4} $$

where

$$ \begin{aligned} \text{sign}(x_j - x_k) &= 1 \text{ if } x_j - x_k > 0 \\ \text{sign}(x_j - x_k) &= o \text{ if } x_j - x_k = 0 \\ \text{sign}(x_j - x_k) &= -1 \text{ if } x_j - x_k < 0. \end{aligned} $$

A very high positive value of S implies an upward trend, whereas a lower negative value indicates a downward trend. To statistically assess the importance of the trend, however, the probability associated with S and the sample size, n, must be computed. Furthermore, we applied a simple nonparametric approach to determining the size of a time series trend as per (5). The trend is determined by [52]

$$ \beta = \text{Median}\left(\frac{x_j - x_i}{j - i}\right), \quad j > i \tag{5} $$

β stands for Sen's slope estimate. $\beta > 0$ shows a positive (upward) trend in a time series, and contrary, $\beta < 0$ indicates a negative (downward) trend over a time series.

The current study used the R Studio for ΔGWS SLT decomposition, SPI calculation, Mann–Kendall trend, and Sen's slope tests.

E. GRACE-Derived GWSD

The hydrological features are shown by the monthly GWS deficit (GWSD) using the following equation [53]:

$$ \text{GWSD}_{i,j} = \Delta\text{GWS}_{i,j} - \Delta\overline{\text{GWS}}_{j} \tag{6} $$

where $\mathrm{GWSD}_{i,j}$ and $\Delta\mathrm{GWS}_{i,j}$ are GWSD and ΔGWS for the jth month in the year i, respectively, and $\Delta\overline{\mathrm{GWS}}_j$ is the long-term mean of ΔGWS for the jth month. GWS is less than the normal value if the GWSD is negative. The GWSD index (GWSDI) is the normalized GWSD calculated using the zero mean normalization approach, as stated in the following:

$$\mathrm{GWSDI} = \frac{\mathrm{GWSD} - \mu}{\sigma}. \tag{7}$$

The mean and standard deviation of the GWSD time series, respectively, are μ and σ.

The current study calculated and plotted the monthly time series analysis of GWSD and GWSDI derived from GRACE deseasonalized ΔGWS from April 2002 to October 2021 over the five major river basins of Afghanistan with unit millimeter (mm).

F. Groundwater Storage Abstraction

Variations in GWS (ΔGWS) are assumed to be equal to the difference between recharge (R) and GWS abstractions ($\mathrm{GWS}_{\mathrm{abs}}$) at a regional scale as follows [39]:

$$\Delta\mathrm{GWS} = R - \mathrm{GWS}_{\mathrm{abs}}. \tag{8}$$

The involved factors for groundwater recharge are precipitation (P), actual evapotranspiration (AET), SWS, and ΔSM through the water budget equation (9) [54].

While the case of groundwater recharge in Eastern and Central highland Afghanistan is influenced by snow-melted water and precipitation, the Western and Southern Afghanistan groundwater recharge can be strongly influenced by percolation in irrigated areas. As agriculture plays a significant role in the country's economy, estimating groundwater recharge efficiency in irrigated areas is a practical approach and a significant "food for thinking" to be taken up in detail by future studies

$$R = P - \mathrm{AET} - \mathrm{SWS} - \Delta\mathrm{SM}. \tag{9}$$

$\mathrm{GWS}_{\mathrm{abs}}$ was calculated by using the following equation as applied by [54]:

$$\mathrm{GWS}_{\mathrm{abs}} = P - (\mathrm{AET} + \mathrm{SWS} + \Delta\mathrm{SM} + \Delta\mathrm{GWS}). \tag{10}$$

In this study, we calculated the spatial distribution of recharge value for the entire country by subtracting the AET, SWS, and change in SM (ΔSM) from total precipitation provided by CHIRPS. Furthermore, the abstracted GWS has been calculated in a unit (km) and multiplied by the pixel area (25×25 km) to estimate the abstracted GWS volume in cubic kilometers. The $\mathrm{GWS}_{\mathrm{abs}}$ rate has been calculated by dividing the total abstracted volume by the number of years with unit km^3/year. The positive value indicates decreasing GWS; conversely, the negative value indicates a positive recharge balance.

G. Land Deformation Detection by InSAR

The current study used the Sentinel-1 data (C-band) to detect the land deformation in Kabul using the Generic Mapping Tools Interferometric SAR (InSAR) Processing System (GMTSAR), Sentinel Application Platform (SNAP), and Statistical-cost Network-flow Algorithm for Phase Unwrapping (SNAPHU) tools. We considered 28 scenes of descending orbit for time series analysis by GMTSAR from 2015 to 2020. Parallelly, four scenes (two ascending and two descending) were used for decomposing to vertical and horizontal displacements by SNAP and SNAPHU.

Two complicated SAR images are combined to form an interferogram. An InSAR interferogram (γ) is a picture created by subtracting two co-registered SAR phase images of the same region using (11). It is defined as the normalized complex correlation coefficient of the complex electromagnetic fields S_1 and S_2 backscattered by the lit elements at positions ρ_1 and ρ_2 [55]

$$\gamma = \frac{\langle S_1 S_2 * \rangle}{\langle S_1 S_1 * \rangle \langle S_2 S_2 * \rangle}. \tag{11}$$

Here, the bracket $\langle S \rangle$ is the average of S, and $S*$ is the complex conjugate of S.

The path difference is measured using the interferometric phase difference using the following equation:

$$\varphi = \varphi_1 - \varphi_2 = \frac{4\pi}{\lambda}[\rho_1 - \rho_2]. \tag{12}$$

Here, φ_1 and φ_2 are phases of the first and second SAR images, respectively, and φ is the interferometric phase. ρ_1 is the first acquisition's distance from the SAR sensor to the scatterer; ρ_2 is the second acquisition's distance, and λ is the wavelength.

Differential interferometry (D-InSAR) offers information on changes in the range distance between the sensor and the ground target due to the ground target's displacement [56], [57]. The objective of D-InSAR is to measure ground deformation through repeat-pass interferometry. In this method, LOS displacements directly contribute to the interferogram, irrespective of the baseline, allowing for measurements in terms of a fraction of the wavelength. From distances spanning hundreds of kilometers, the D-InSAR has the capability to detect subtle ground deformations with a precision of several millimeters [58], [59]. The fundamental D-InSAR approach involves removing the phase of topographic displacements, which may be accomplished with an external digital elevation model (DEM) [60]. The DEM is then used to create a synthetic interferogram [61], as shown in (13). Furthermore, atmospheric artifacts can significantly impact differential interferograms [56]

$$\begin{aligned} \Delta\psi_{\mathrm{intf}} &= \Delta\psi_{\mathrm{flat}} + \Delta\psi_{\mathrm{topo}} + \Delta\psi_{\mathrm{mov}} + \Delta\psi_{\mathrm{atmos}} + \Delta\psi_{\mathrm{noise}} \\ \pm n * 2\pi &= \frac{4\pi \cdot B_{\perp} \cdot r}{\lambda \cdot \rho \cdot tg\theta} + \frac{4\pi \cdot B_{\perp} \cdot h}{\lambda \cdot \rho \cdot \sin\theta} + \frac{4\pi \cdot \Delta\rho}{\lambda} + \Delta\psi_{\mathrm{atmos}} \\ &\quad + \Delta\psi_{\mathrm{noise}} \pm n * 2\pi. \end{aligned} \tag{13}$$

Here, $\Delta\psi_{\mathrm{flat}}$ represents the flat Earth component related to range distance, $\Delta\psi_{\mathrm{topo}}$ represents the topographic phase, $\Delta\psi_{\mathrm{mov}}$ represents the component due to terrain displacement in the slant-range direction or LOS between two SAR acquisitions, $\Delta\psi_{\mathrm{atmos}}$ represents the phase related to atmospheric artifacts, and $\Delta\psi_{\mathrm{noise}}$ represents degradation factors such as spatial and temporal decorrelation. $n*2\pi$ represents phase

ambiguity where n is a whole number, such as 1, 2, 3, ..., including zero. Here, λ, $B_{\perp}$, r, h, and $\Delta\rho$ are radar wavelength, look angle, slant-range distance of the master image, normal spatial baseline component of the data pair due to orbital separation, and the topographic height of the given point and ground displacement parallel to the radar LOS, respectively.

Decreasing the interferogram's noise component requires a filter, but it does not enhance or recover the signal [62]. Goldstein filtering is a Goldstein technique modification that increases fringe visibility and lowers noise caused by temporal or baseline-related decorrelation. In Goldstein filtering, alpha is crucial for fine-tuning the filter strength. Alpha is an arbitrary number between zero and one that has the most significant influence on filter performance. The greater the filtration, the higher the alpha value.

When extreme values of $-\pi$ or π are achieved, the extracted phase appears to stop, i.e., the phase jumps to the opposite end. The phase of the radar echoes can only be measured up to 2π, but altitudes require the whole phase at each location in the picture. This 2π uncertainty is resolved by phase unwrapping. Different phase unwrapping technologies have been utilized, such as region expansion, lowest cost flow, and phase decomposition. However, none of them is ideal. Even if the heights are enormous, slow-altering topography is not an issue. If elevations are confined, rough topography is not a concern.

H. Displacement Mapping

Point-based approaches are costly and ineffective for monitoring vast deformation regions [63]. As a result, D-InSAR is a crucial approach for accurately measuring displacement. Moving half of a wavelength for the pixel and a round-trip distance wavelength for the radar signal generates one fringe, or a 2π phase difference, in the range direction. As a result, one entire phase cycle or fringe in a D-InSAR Interferogram indicates a radar LOS ground displacement of $\lambda/2$, where λ is the wavelength of the radar microwave pulse employed. Sentinel-1 (C-band) radar data (5.6 cm wavelength) were employed in this study, which indicates that each displacement fringe represents a minimum displacement of 36.11 mm, as determined for the C-band European Remote Sensing (ERS) SAR satellite, equal to 30.42 mm by [64] using the following equation:

$$\frac{\frac{\lambda}{2}}{\mathrm{Cos}\theta} = \frac{\frac{56\mathrm{mm}}{2}}{\mathrm{Cos}(39.16^{\circ})} = 36.11\mathrm{mm}. \tag{14}$$

If a region on the ground is displaced by Δr in the LOS direction of the radar, the path difference between the two acquisitions, $2\Delta r$, phase of $\Delta\Phi$ given by the following:

$$\Delta\boldsymbol{\Phi} = \left(\frac{\mathbf{4}\pi}{\lambda}\right)\Delta r. \tag{15}$$

We need to find the displacement direction to understand the nature of the movement. Therefore, we decomposed the LOS displacement into vertical and horizontal displacement. The interferometric observation can naturally see the only motion in the SAR LOS direction, but there may be some ambiguities in LOS measurements. To measure the 3-D displacement, we require at least three independent LOS. Since the global navigation satellite system (GNSS) is not available for this study area, we processed two independent radar LOSs (ascending and descending passes) over the same spatial and temporal extent. We note that both the ascending and descending directions are at highly steep angles in the case of Sentinel-1 dataset (i.e., swath 1) ($\sim$34° from the normal). We can quantify horizontal motion only along the east–west axis precisely since the north component is insensitive in SAR measurement [65]. The vertical and east–west decomposition is derived based on the simple geometric principle [66], [67] using the following equations:

$$d_{\mathrm{EAST}} \approx \frac{(d_{\mathrm{LOS\_Desc}} - d_{\mathrm{LOS_{Asc}}})/2}{\sin(\theta)} \tag{16}$$

$$d_{Z} \approx \frac{(d_{\mathrm{LOS\_Desc}} + d_{\mathrm{LOS_{Asc}}})/2}{\cos(\theta)} \tag{17}$$

where d is displacement along the respective components and θ is the incident angle.

To retrieve the east–west and vertical displacement, we used the ascending and descending orbits SAR images from June 2016 to August 2020. We used SNAP along with SNAPHU plugin to process the vertical and horizontal displacement decomposition.

The whole workflow process and methodology are shown in Fig. 3.

IV. Results and Discussion

A. SPI-Based Drought Analysis and Seasonal GWS Change

The SPI was calculated from CHIRPS monthly rainfall data over five river basins from 2003 to 2021. The SPI analysis result is presented in Fig. 4. The drought intensity has been determined according to [47], which is classified in Table III and compared with the seasonal GWS variation.

The result shows positive values in 2003 for all river basins, excluding the Kabul basin. However, the values are almost between (+1.5 and −1), indicating a moderately wet to near-normal condition. In 2004, the whole country was affected by a drought. Kabul, Northern, and Helmand basins are facing an arid period, but the Amu Darya and Hari Rud basins faced severe drought in 2004. This drought has affected GWS that is visible in seasonal GWS change and SPI time series analysis (see Fig. 4). The result does not show any significant drought between 2005 and 2007 over all the basins. Though the Kabul basin faced a moderate drought in 2006, other basins faced near-normal conditions. During 2008, all five basins showed negative SPI with severe drought conditions, which is more visible for Hari Rud and Helmand basins than the other three basins. The SPI is showing an improvement between 2009 and 2010 compared to adjacent years. From 2011 to 2014, a continuous drought was recorded that accelerated the negative trend of GWS change in Kabul, Amu Darya, and Northern basins. In contrast, the two other basins show this negative acceleration from the end of 2007 to 2008. The SPI shows more or less near-normal conditions over the whole country from 2015 to 2017, but at the end of 2017 and 2018, there

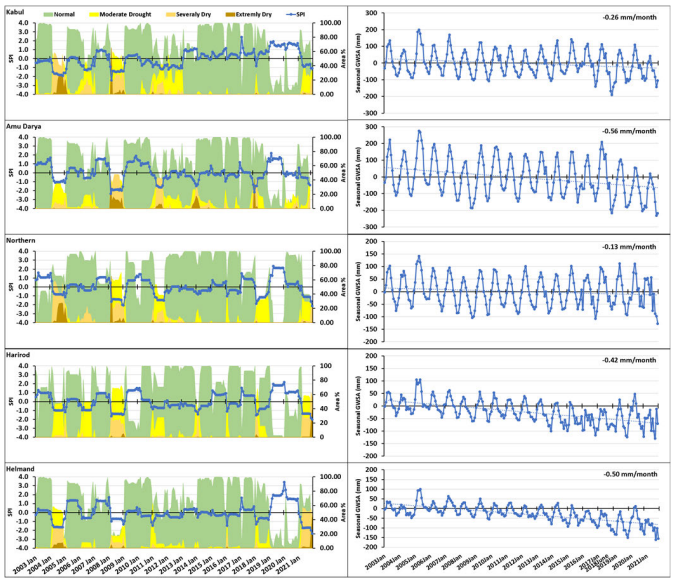

Fig. 4. (Left side) SPI time series analysis shows the drought occurrence and (right side) ΔGWS with the trend line for the five river basins from 2003 to 2021.

was moderate drought with high intensity in the south and southwest parts of the country. During 2019 and 2020, the SPI increased due to sufficient rainfall over the whole country, excluding the northern part (Amu Darya and Northern basins), where it showed normal conditions in 2020. From the end of 2020 to 2021, the country is going through moderate to extreme drought with maximum intensity in the south and west parts (Hari Rud and Helmand basins).

B. Groundwater Trend Analysis

To understand the groundwater trend, the Mann–Kendall trend test (M–K test) and Sen's slope test have been applied to a dataset of 225 months (the entire time interval of the study) using the R studio software. The mathematical explanation is given in (4) and (5). The result shows a negative value (decreasing trend) for both tests (M–K and Sen's slope) for all the river basins. It indicates that the country is going through a shortage of GWS. All the negative signs of Kendall's Tau and Sen's slope test prove a decreasing trend. The likelihood of getting the observed results, given that the null hypothesis is true, is measured by a p-value. The statistical significance of the observed difference increases as the p-value decreases. Statistical significance is commonly defined as a p-value of 0.05 or less. The p-value < 0.05 indicates the trend is monotonic (it signifies that the variable continuously rises (down) with time, although the trend is not always linear), as shown for the Kabul and Amu Darya basins. On the contrary, the p-value > 0.05 indicates that the trend is away from monotonic, as shown for the Northern, Hari Rud, and Helmand basins, but it is still decreasing according to Sen's slope value. The details are given in Table IV.

The regional GWS time series range amplitude has been reduced by removing the seasonal effects after decomposition. Thus, seasonal effects can be determined by subtracting the deseasonalized and original trends for each basin (see Table V).

TABLE IV

MANN KENDALL TREND AND SEN'S SLOPE TESTS INDICATE A DECREASING TREND OVER THE FIVE BASINS FROM 2002 TO 2021

Name of Basins	Scores (S)	Z-Value	P-Value	Kendall's Tau	Trend	Sen's Slope
Kabul	-3262	-2.88912	0.00386	-0.12944	Decreasing	-0.202
Amu Darya	-4784	-4.23756	0.00002	-0.18984	Decreasing	-0.477
Northern	-1780	-1.57613	0.11500	-0.07063	Decreasing	-0.082
Hari Rud	-11524	-10.20894	0.00000	-0.45730	Decreasing	-0.392
Helmand	-13276	-11.7612	0.00000	-0.52683	Decreasing	-0.458

TABLE V

DECOMPOSED GWS CHANGE TRENDS COMPARED TO THE SEASONAL TREND OVER THE FIVE BASINS

Trend		Cold, Dry Summer		Arid, Steppe		Arid, Desert
		Kabul	**Amu Darya**	**Northern**	**Hari Rud**	**Helmand**
Regional (Seasonal) ΔGWS Trend in Flux (mm/month)		-0.26	-0.56	-0.13	-0.42	-0.50
Short-Term Trend (Deseasonalized)	Trend in flux (mm/month)	-0.22±0.001	-0.47±0.0003	-0.09±0.0004	-0.38±0.0004	-0.46±0.0003
	Trend in mass (km^3/month)	-0.016	-0.042	-0.007	-0.039	-0.138
Long-Term Trend (Deseasonalized)	Trend in flux (mm/year)	-2.464	-4.799	-0.682	-4.347	-5.422
	Trend in mass (km^3/year)	-0.172	-0.426	-0.053	-0.432	-1.583

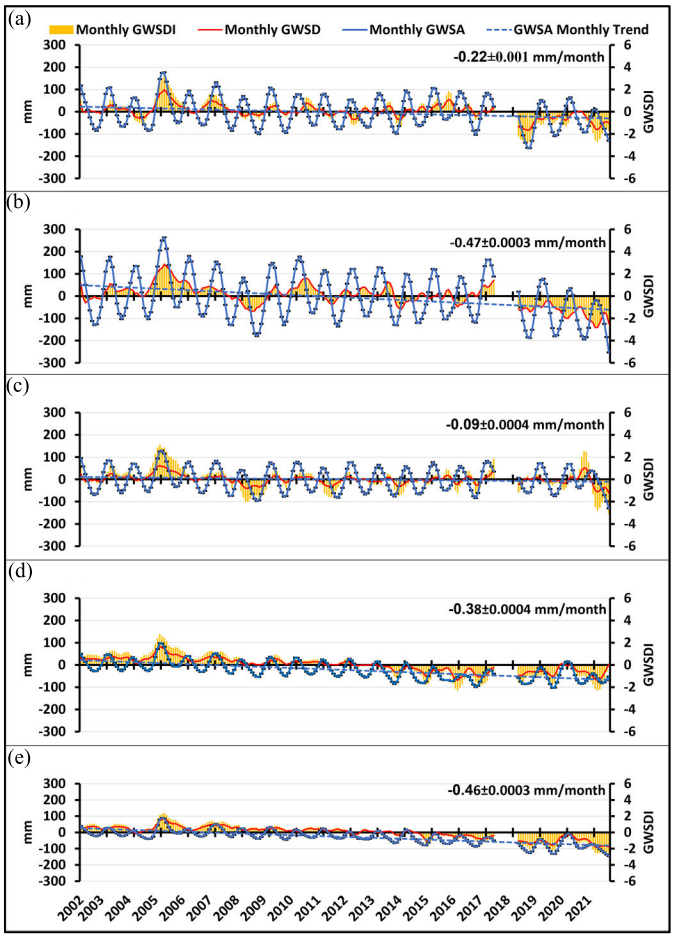

Fig. 5. Deseasonalized groundwater storage change with GRACE uncertainty, GWSD, and GWSDI time series over five river basins from 2002 to 2021. (a) Kabul basin. (b) Amu Darya basin. (c) Northern basin. (d) Hari Rud basin. (e) Helmand basin.

The GWS change trend in flux has been calculated for both short term (mm/month) and long term (mm/year), as shown in Table V. In addition, we have calculated the GWS trend in mass in both long term (km^3/year) and short term (km^3/month) for all the basins. The maximum long-term decreasing trend has been identified for the Helmand basin, primarily arid desert areas. According to previous research and reports, the dramatic depletion of groundwater in the southern region of Afghanistan is affected by recent regional and global climate change, temperature increases, and excessive groundwater abstraction for irrigation purposes. The GWS change time series analysis shows that all the basins are going through a declining phase with maximum trend value for the Amu Darya and Helmand basins, followed by Hari Rud, Kabul, and Northern basins. Overall, the turning point of groundwater decline in Afghanistan was observed in 2008, which is significantly raised in the northern part of the country. The south part reached the turning point earlier in 2005–2006. The GWS change that ranges from 2002 to 2021 for each basin is Kabul (177 to −163 mm), Amu Darya (246 to −253 mm), Northern (129 to −130 mm), Hari Rud (89 to −102 mm), and Helmand (89 to −146 mm).

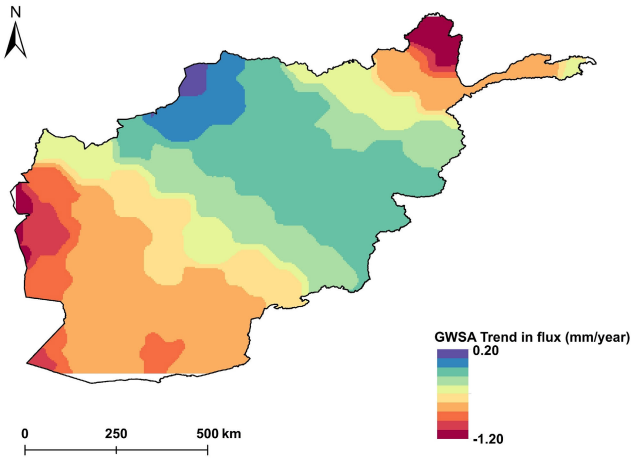

Fig. 6. Long-term trend map of GWS Anomaly in Afghanistan between 2002 and 2021.

C. GWS Deficit

The GWSD and GWSDI have been calculated for all five river basins. The negative index signifies a shortage of GWS (less than the normal value). Fig. 5 shows a higher negative GWSDI for Kabul and the Amu Darya basins after 2018. In contrast, the other three basins consistently go through a similar higher negative GWSDI from 2011 to 2021. The result reveals a significant groundwater drought in the Kabul and Amu Darya basins after 2018, whereas the other three river basins faced groundwater drought for over a decade since 2011. The reasons for the spread of the drought are mainly due to the poor recharging of the groundwater reservoirs from the available surface water and precipitation because the rainfall fluctuations are not significant over the same period. Although the GRACE data account for the TWS due to the melted water, including glaciers, it was not consistent over the five river basins. Therefore, we only attributed the reasons for drought to the surface water from rainfall and snow-melted water. Hence, the reasons for the observed drought concerning ΔGWS (see Fig. 4) in the area can be safely attributed to anthropogenic factors.

We also noticed some other short-period deficits while performing the time series analysis of GWSD data, but it is primarily inconsistent and insignificant. The monthly deseasonalized ΔGWS trend in flux is represented along with GWSD and GWSDI for all river basins in Fig. 5.

The long-term spatial trend of ΔGWS is calculated for the entire country, which eases to identify the regions with less sustainability (see Fig. 6).

D. Groundwater Abstraction and Mass Loss

GWS_{abs} has been driven using a recharge and discharge balance equation from GRACE, GLDAS, MODIS, and CHIRPS datasets using (10). This process aims to understand how much groundwater has been withdrawn from the subsurface. The GWS_{abs} trend in flux (mm/year) spatial distribution is represented in Fig. 7. The maximum abstraction has been determined in the northeast and southwest parts of the country (12.60 mm/year). GWS_{abs} in Northern basin is less due to

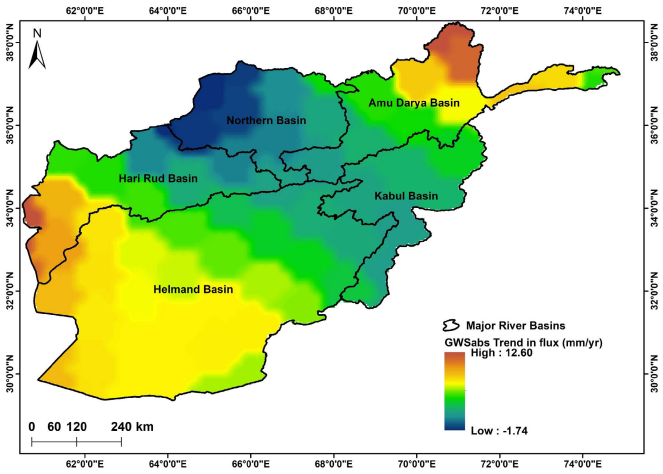

Fig. 7. GWS_{abs} trend in flux (mm/year) over the entire country from 2003 to 2021. The positive value indicates groundwater abstraction.

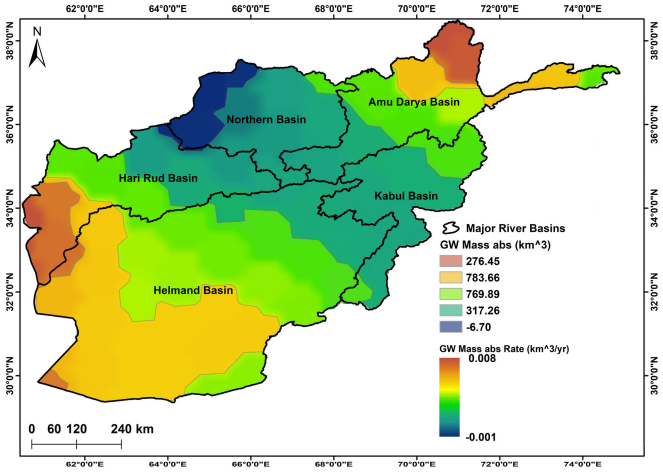

Fig. 8. GWS_{abs} trend in mass (km^3/year) and abstracted volume of groundwater (km^3) from 2003 to 2021.

sufficient precipitation and a low drainage system on flat topography.

The GWS_{abs} trend in mass (km^3/year) and the absolute value for abstracted volume (mass) of GWS in km^3 are calculated by multiplying the area of a pixel (25 × 25 km). The GWS_{abs} trend in mass is shown by color ramp, and the absolute GWS_{abs} has been discriminated by light color boundary, as shown in Fig. 8.

A spatiotemporal analysis for GWS_{abs} change has been done and shown in Fig. 9, showing the temporal variation of GWS_{abs} from 2003 to 2021. The maximum positive abstraction rate was determined in 2021 (up to 23.12 mm toward brown color). Overall, the considerable amount of GWS_{abs} is determined in the country's southwest, southeast, and northeast parts. The minimum value is for the central part, including the Northern basin, with the same recharge window. It can be inferred that a sufficient yearly recharge in the central and northern parts controls a normal abstraction. However, the result shows that the other parts of the country receive insufficient precipitation and lose moisture due to high evapotranspiration with increasing temperature and groundwater demand for irrigation. The

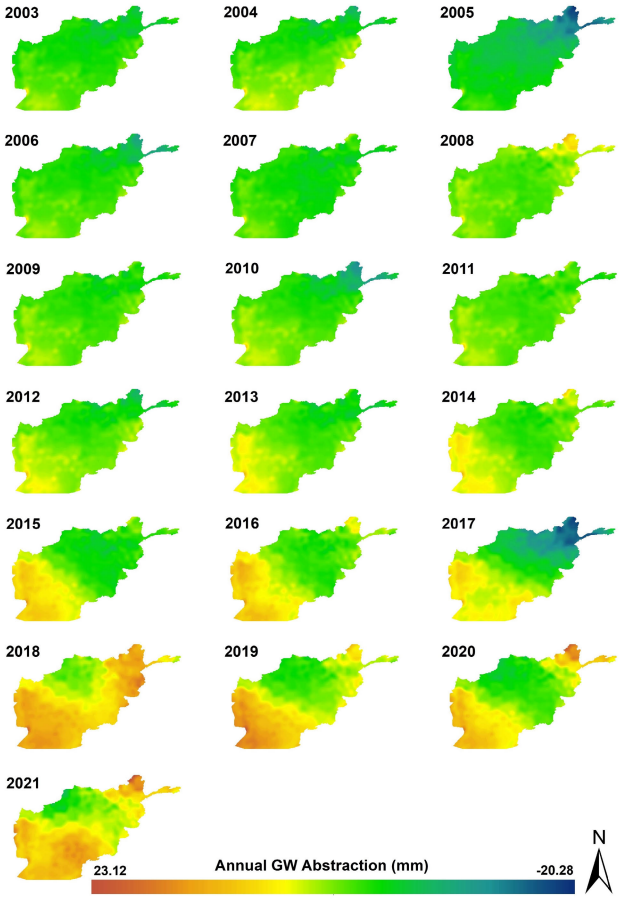

Fig. 9. Spatiotemporal analysis of GWS_{abs} (annual average) over the entire country from 2003 to 2021.

study shows the high groundwater demand in Kabul, Helmand, and Hari Rud basins. The extensive GWS_{abs} in the southern region of the country could be attributed to climate change and an increase in demand for groundwater due to a decrease of precipitation and surface water supply. Despite this, there is no information available on groundwater abstraction rate in Afghanistan. The output of this study can be justified if we assess the ΔGWS and climatic factors. The spatiotemporal ΔGWS and SPI have been assessed in Fig. 4, which show a negative trend after 2012 in Helmand and Hari Rud basins. A similar pattern is determined in GWS_{abs} as well. Therefore, the highly abstracted region in the southern region is mainly affected due to climate change, which could be accelerated by the overextraction of groundwater as well.

E. Land Deformation and Vadose Zone Evolution in Kabul

The excessive groundwater exploitation in Kabul leads to the evolution of the subsurface vadose zone. The geological setting of Kabul made it suitable for urbanization. The city is on a graben filled with unconsolidated sediments capable of groundwater occurrence. Due to the last two decades of population growth in Kabul, the demand for groundwater has also increased. The mismanagement of groundwater extraction has led to a dramatic groundwater level decline in recent years (up to 3-m/year decline was observed in UKBL aquifer from

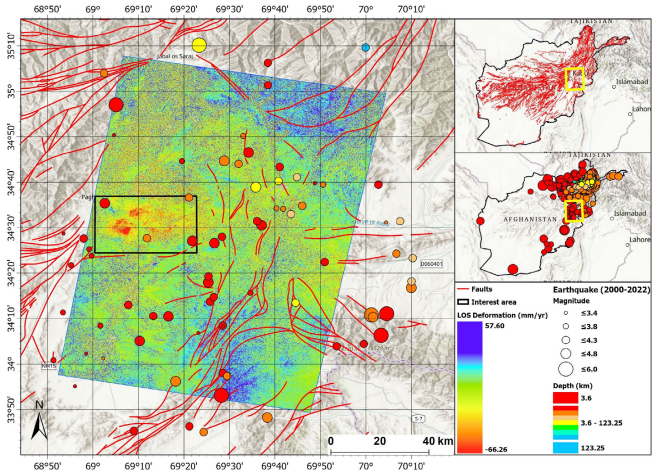

Fig. 10. Average velocity (2015–2020) and seismotectonic map (2000–2022) of the study area to show the potential seismic area and positive deformation region along the major faults and no-fault dominant effects in the negative deformation area.

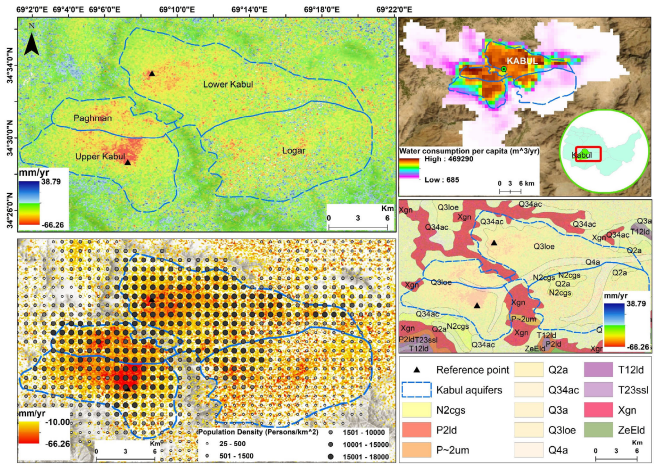

Fig. 11. Deformation velocity map and factors for displacement include population density, water consumption rate, and lithology.

in situ groundwater level data that are correlated with land deformation in Fig. 15). The lithology of Kabul aquifers is mostly clastic alluvial deposits, including gravel, sand, loess, and interbedded clay layers. The land deformation has been determined in Kabul using the D-InSAR technique. An open-source data (Sentinel-1) has been processed for time series analysis from 2015 to 2020 in descending orbit.

The result shows a positive land deformation along the faults, which can be interpreted as tectonic and seismic activity. For the last two decades, the earthquake epicenter has been tracked to understand whether there are any major tectonic events. The map in Fig. 10 shows the most positive deformation along the major faults. The displacement map shows neither significant positive deformation nor fault extension inside the study area (the black rectangle is the Kabul area) in Fig. 10. Therefore, no tectonic activity is involved in this land deformation phenomenon.

Fig. 11 shows the LOS displacement (positive and negative in the upper frame and only negative deformation overlying with population density in the down frame; water consumption

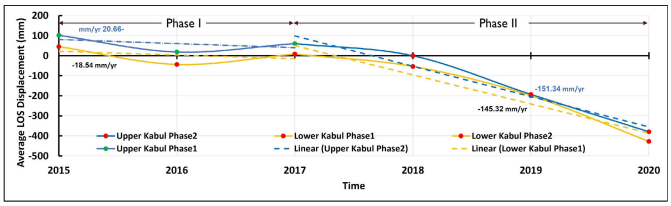

Fig. 12. Time series analysis of LOS displacement in UKBL and LKBL from 2015 to 2020.

map and geological map on the right side). The positive velocity indicates the ground surface movement toward the satellite along the faults. It can be due to seismic activity along the faults in hard rocks. The Precambrian metamorphic bedrocks outcrop along the Asmaye and Sher Darwaza mountains does not show any considerable negative deformation, negligible with green color. It proves the tectonic stability of the area and rejects the hypothesis assuming tectonic activity as the main factor of land deformation in Kabul.

In contrast, negative deformation occurs in unconsolidated sediments (alluvial and loess) dominant area that is assumed to be due to vadose zone evolution (rapid groundwater decline). The spatial distribution of population density and the water consumption rate per capita is plotted following the land deformation pattern, and the population density and water consumption maps indicate that highly populated areas are more affected, which demand more groundwater. The distribution of ground deformation along the LOS follows the four aquifer systems, namely, UKBL PGHMN, LKBL, and Logar aquifers (see Fig. 11). Groundwater is the primary resource of domestic, farming, irrigation, and even factories in Kabul, which has been used extensively in recent years. Despite this, the exact rate of water consumption has not been monitored in Kabul, but the Japan International Cooperation Agency (JICA) estimated 50–60 L/day per capita in 2012 and 100–150 L/day in 2032 [68]. The estimated average water consumption rate map (see Fig. 10) shows the high rate of water consumption in urban areas, which is directly linked to the population density. The spatial distribution and magnitude of land deformation follow the footprint of water consumption in Kabul. Hence, this study correlates the determined land deformation because of vadose zone evolution due to groundwater overpumping and unconsolidated lithology.

We plotted a time series analysis of LOS displacement velocity between (2015 and 2020) at two reference points from UKBL and LKBL within the two phases. The first phase (2015–2017) shows a gentle trend (−20.66 mm/year in UKBL and −18.54 mm/year in LKBL), but the second phase (2018–2020) shows a large trend (−151.34 mm/year in UKBL and −145.32 mm/year in LKBL), as shown in Fig. 12.

The acceleration of land deformation after 2018 could be a topic to discuss from many aspects, including frequent occurrence of earthquakes in the region that can facilitate on porose compaction in vadose zone. This scenario has not been proven yet due to the absence of a successive monitoring system for aquifer compaction such as extensometer. Hence, this research found a moderate meteorological drought period with high intensity over the country in 2018, which is represented in

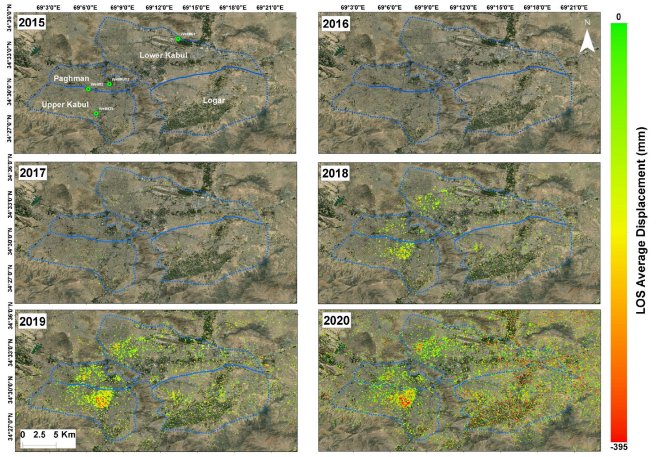

Fig. 13. Spatiotemporal analysis of LOS displacement processed by GMTSAR from 2015 to 2020. The green points feature shows the location of feature points used for correlation with groundwater level.

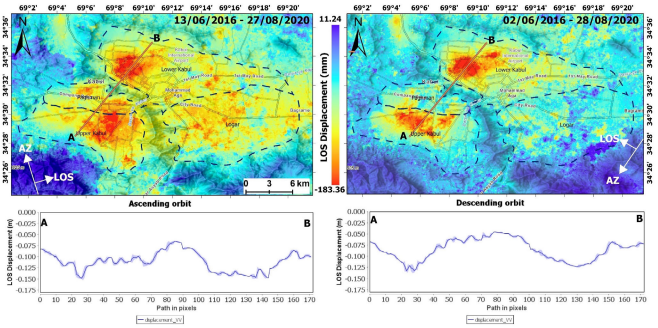

Fig. 14. LOS displacement for (left) ascending orbit and (right) descending orbit with respective cross sections.

Fig. 4. The spatiotemporal analysis of groundwater abstraction also indicates a high extension of abstraction in Helmand and Kabul basins after 2018 that could be inferred as increased on groundwater consumption. The in situ groundwater level data from the monitoring well show a dramatical decline between 2018 and 2019 (∼6 m) observed in UKBL aquifer, while the average decline was (3 m/year), as shown in Fig. 16. Therefore, the authors infer that drastic trend of land deformation after 2018 could be due to dramatic decline in groundwater level as a result of interplay impacts of anthropogenic and climatic factors.

The annual average deformation map does not show considerable displacement before 2018, but from 2018 to 2020, the deformation patches are developing. The maximum LOS displacement is recorded at −395 mm up to 2020 in UKBL, specifically in Darul-Aman and Afshar regions (see Fig. 13).

This study retrieved the vertical and east–west displacement components by combining the LOS displacement estimated from Sentinel-1 ascending and descending tracks. The LOS displacement for ascending and descending orbits has been drawn between single pairs for each orbit from June 2016 to August 2020, as shown in Fig. 14. However, the spatial distribution of deformation patches is not the same for ascending and descending due to the satellite-looking angle direction, but

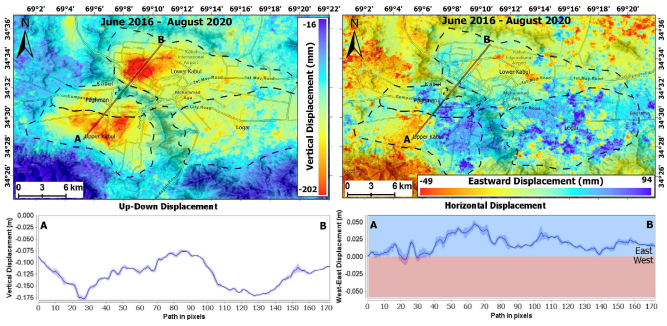

Fig. 15. Decomposition of LOS displacement to (left) vertical component and (right) east–west component and their respective cross sections.

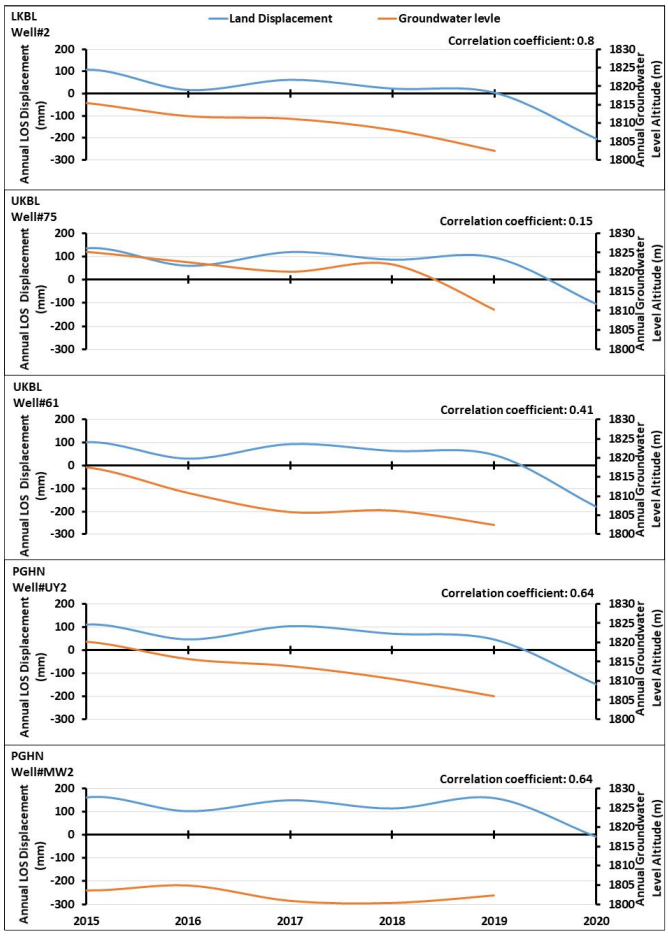

Fig. 16. Time series analysis of annual land displacement and GWL fluctuation for four reference points in LKBL, UKBL, and PGHMN aquifer system from 2015 to 2020. The GWL data are provided by the Ministry of Energy and Water (MEW) up to 2019.

the descending LOS displacement processed by SNAP shows similar patches to that of GMTSAR.

This study focuses on land deformation resulting from groundwater exploitation and vadose zone evolution, so the vertical and horizontal displacements are discriminated by combining two LOS displacements. The result shows up to a maximum (−202 mm) vertical displacement in UKBL and LKBL aquifers, the most populated area in Kabul, from June 2016 to August 2020 (see Fig. 15). A cross section (A–B) indicates the sharpest vertical displacement in Western Kabul.

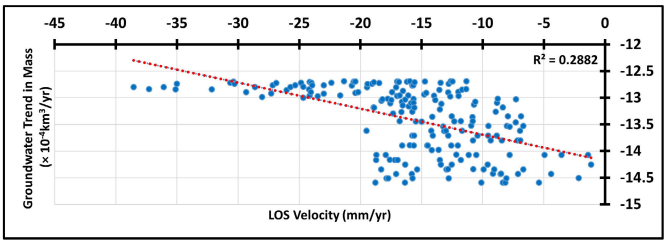

Fig. 17. Correlation between land deformation and groundwater mass loss derived from GRACE.

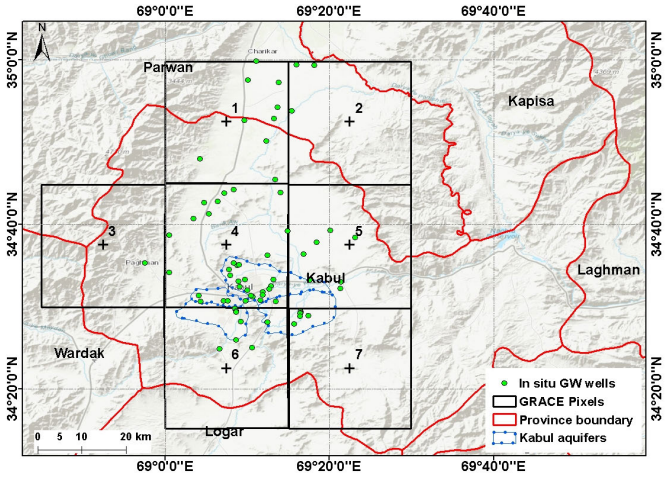

Fig. 18. GRACE pixel and in situ groundwater wells are plotted over Kabul and adjacent districts.

The east–west displacement is calculated similar to vertical displacement. The positive value (blue) indicates an eastward movement, while the negative value (red) shows the westward displacement.

F. Data Validation and Correlation

The GWL fluctuation and land displacement are plotted together in Fig. 16. It is difficult to find the exact pattern for these two phenomena because different physics and mechanisms govern them. Even if we consider the land deformation to be driven by groundwater exploitation only, it will still not follow the same cycle because the GWL decline and replenishment can easily be a high-frequency phenomenon and can change value much more rapidly than the observed land deformations.

Land deformation is not a straightforward understanding and may have several factors contributing to it. In places, it could simply be the increasing overburden without much strength in the subsurface formations to support the same. In contrast, in other places, it could be the weakening of the subsurface formation and their arrangement due to some channels cut or some processing responsible for vadose zone development, resulting in the weakening of lithology. The only other reasons for land deformations are the local tectonic activities, but we have comprehensively ruled out such a situation because our analysis of the tectonic framework around the city revealed no such major active faults and lineament along which such a land deformation could have occurred in the unconsolidated lithological units, particularly

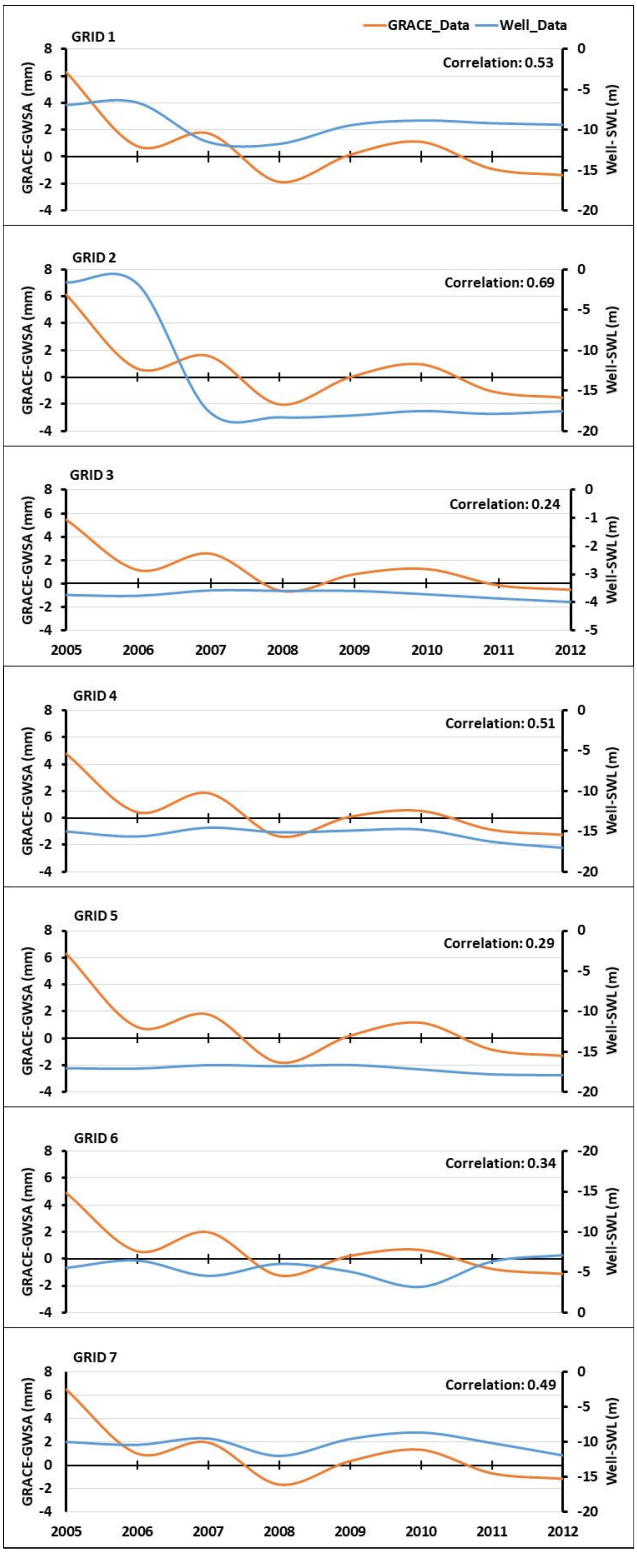

Fig. 19. Graphical representation from Grid 1 to Grid 7 shows the correlation between the annual average of ΔGWS derived from GRACE and GWL from in situ data provided by USGS and AGS [69] between 2005 and 2012 in Kabul. The graphs are plotted regarding GRACE water equivalent thickness (mm) and groundwater SWL (m). The pixels and well locations are shown in Fig. 18.

when compared to the hard terrain in the surrounding region that did not also show any significant displacement. On the other hand, land deformation is a slow process rather than

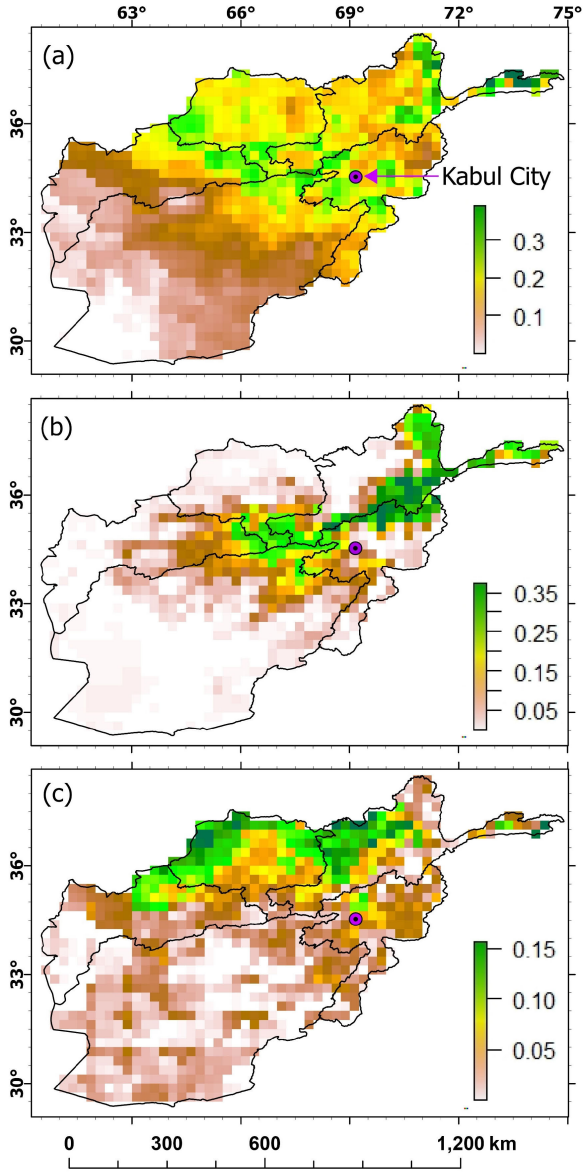

Fig. 20. Spatial correlation of GWS with (a) RAINFALL, (b) SMEW, and (c) SWS.

a GWL drawdown. Therefore, in this case, we can see both phenomena following a similar pattern showing a relationship between GWL fluctuation and land deformation, as shown in Fig. 16. The GWL data are available up to 2019, and displacement is plotted up to 2020.

The correlation between land deformation and GRACE-derived groundwater mass loss was plotted. Though the correlation coefficient is not a higher value, there is still a positive correlation (see Fig. 17).

Due to the low number of in situ wells data in Afghanistan, there was only groundwater well data available from 2005 to 2012, a groundwater monitoring well network that the United States Geological Survey (USGS) and Afghanistan Geological Survey (AGS) established in 2004. The spatial distribution of 70 groundwater wells and seven GRACE pixels is shown in Fig. 18. A sufficient number of monitoring wells in pixels 1, 2, 4, and 6 show a greater than 0.5 correlation coefficient between GRACE-derived GWS and in situ SWL. The graph pattern is similar to the rest of the pixels, but due to the poor distribution of monitoring wells, the correlation coefficient is less than 0.5, as shown in Fig. 19.

The spatial correlation between hydrological components and ΔGWS has been calculated for the whole dataset (raster files) using the R studio from 2002 to 2021. The result shows that SMEW and GWS have a reasonable correlation in the northeast and central highlands along the Pamir, Hindukush, and Baba mountains [see Fig. 20(a)]. The rainfall and GWS moderately correlate in Kabul, Amu Darya, and Northern basins [see Fig. 20(b)]. The SWS shows a good correlation with GWS in the north part of the country, which could be due to the Amu and Kunduz rivers' gentle topography and wide-spreading paths having a sufficient contribution to groundwater recharge [see Fig. 20(c)]. In the south and west parts of the country (Hari Rud and Helmand basins), there is no significant correlation with any of the components, which could be due to not the presence of snowfall in the south region and also less amount of rainfall.

V. Conclusion

Afghanistan is a landlocked country with a semiarid to arid climate and mostly depends on groundwater for various purposes in the context of water supply. Unfortunately, due to the unstable political situation and nonimplementation of the available technology, there is a limited groundwater monitoring network in major cities with wide data gaps. Therefore, for understanding the long-term scenario over the whole country, continuous data recording is critical to indicate and investigate the key factors for groundwater fluctuation.

Due to past droughts and increased groundwater demand, most parts of the country suffer from severe groundwater stress. The SPI value showed a severe drought in 2005, 2008, and 2011 that was also detected in seasonal GWS time series analysis. However, the SPI value significantly improved between 2015 and 2020, excluding 2018. A negative seasonal GWS variation trend has been determined from 2008 to 2011. The spatial distribution of drought severity gradually increases over Kabul, Amu Darya, Northern, Hari Rud to Helmand basins. To understand the long-term trend, the seasonal components were removed using the LOESS function. A Mann–Kendall trend and Sen's slope tests were applied for deseasonalizing GWS anomalies. The trend analysis reveals the decreasing trend for all the basins with negative values of Kendall's tau (T) and Sen's slope (β): Kabul ($T = -0.12944$ and $\beta = -0.202$), Amu Darya ($T = -0.18984$ and $\beta = -0.477$), Northern ($T = -0.07063$ and $\beta = -0.082$), Hari Rud ($T = -0.45730$ and $\beta = -0.392$), and Helmand ($T = -0.52683$ and $\beta = -0.458$).

The GWS_{abs} trend in flux determined for 2003–2021 showed a maximum value of 12.60 mm/year for the northeast and southwest parts of the country, whereas the north and central regions along with the east part of the country mostly showed comparatively a low rate of GWS_{abs}.

The severe groundwater stress was concentrated in the country's southern and western regions. The contributing

factors could be insufficient precipitation, high temperature, and increased groundwater demand for irrigation in recent years. The effects of groundwater decline and the evolution of the vadose zone on land deformation in Kabul have been determined using Sentinel-1 data and the InSAR technique from 2015 to 2020. A considerable vertical land deformation (maximum to −202 mm subsidence) was observed in UKBL followed by other zones of PGHMN and LKBL aquifer systems. Other factors, such as lithology, tectonics, and population, were also evaluated, and it was found that densely populated and unconsolidated sedimentary areas mostly dominated the rate and spatial distribution of land deformation. Finally, GRACE ΔGWS and InSAR-derived land deformation have been correlated with in situ wells data. It showed a strong positive correlation between GWL fluctuation and ΔGWS.

Data Availability

Interferometric SAR data have been downloaded from the ALASKA-NASA Earth Data portal (ASF) that has been remotely sensed by the Sentinel-1 A satellite (https://search.asf.alaska.edu/#/). GLDAS Noah Land Surface Model L4 monthly 0.25° × 0.25° V2.1 (GLDAS_NOAH025_M) downloaded from https://disc.gsfc.nasa.gov/datasets/GLDAS_NOAH025_M_2.1. The "CSR_GRACE_GRACE-FO_RL06_Mascons_all-corrections_v02" and "CSR_GRACE_GRACE-FO_RL06_Mascons_v02_LandMask" datasets have been downloaded from http://www2.csr.utexas.edu/grace. The monthly precipitation (CHIRPS data) has been downloaded from https://data.chc.ucsb.edu/products/. The AET dataset (Processed from MODIS) has been provided by the United States Geological Survey (USGS) FEWS NET Data Portal (https://earlywarning.usgs.gov/fews/product/468). Geological data has been created from the Russia Geological Survey map that has been digitized by the USGS (https://certmapper.cr.usgs.gov/data/apps/world-maps/). The Seismicity data has been downloaded from https://earthquake.usgs.gov/earthquakes/search/. The Kabul City population density dataset with 1-km spatial resolution has been downloaded from the ESRI ArcGIS Online Server (https://www.arcgis.com/sharing/rest/content/items/8c9572389dd8476ea541c33f343b3a8f). The in situ groundwater level data of Kabul for the period of 2015–2019 have been provided by the Ministry of Energy and Water (MEW), Afghanistan, and from 2005 to 2012, it was provided by USGS and Afghanistan Geological Survey (AGS).

Author Contributions

Mohammad Taqi Daqiq: the conception of the original problem, complete first draft, designed and customized workflows, executed results and explanations, and detailing illustrations. Ravi Sharma: original idea, guidance, correction and flow of manuscript, and edits. Anuradha Karunakalage: helped in workflows, processing of results, and discussions. Suresh Kannaujiya: the conception of the original idea and problem statement, helped the first author to design workflow and draft modifications.

Acknowledgment

The authors appreciate and offer their special thanks to the Afghanistan Geological Survey (AGS), the United States Geological Survey (USGS), and the Ministry of Energy and Water (MEW) for helping them by providing groundwater level data, ESA for providing the Sentinel-1 data and SNAP software, NASA for providing Gravity Recovery and Climate Experiment (GRACE), GRACE/Following (FO), and Global Land Data Assimilation System (GLDAS) data, Climate Hazard Center, UC Santa Barbara, for providing Climate Hazards Group Infrared Precipitation with Stations (CHIRPS) data, USGS for providing the actual evapotranspiration (AET) and geological data, and ArcGIS Online Server for providing the population density data. They acknowledge ESRI for providing ArcGIS Desktop and ArcGIS Pro software and the National Science Foundation Geoinformatics Program, Scripps Institution of Oceanography, and San Diego State University for providing the GMTSAR. They are grateful to the Institute Computer Center (ICC), Indian Institute of Technology Roorkee, Roorkee, India, for helping them by providing all required licensed software and processing system.

References

[1] W. Aeschbach-Hertig and T. Gleeson, "Regional strategies for the accelerating global problem of groundwater depletion," *Nature Geosci.*, vol. 5, no. 12, pp. 853–861, Dec. 2012, doi: 10.1038/ngeo1617.

[2] R. G. Taylor et al., "Ground water and climate change," *Nature Climate Change*, vol. 3, no. 4, pp. 322–329, Apr. 2013, doi: 10.1038/nclimate1744.

[3] M. Rodell, I. Velicogna, and J. S. Famiglietti, "Satellite-based estimates of groundwater depletion in India," *Nature*, vol. 460, no. 7258, pp. 999–1002, Aug. 2009, doi: 10.1038/nature08238.

[4] W. Feng, M. Zhong, J. Lemoine, R. Biancale, H. Hsu, and J. Xia, "Evaluation of groundwater depletion in North China using the Gravity Recovery and Climate Experiment (GRACE) data and ground-based measurements," *Water Resour. Res.*, vol. 49, no. 4, pp. 2110–2118, Apr. 2013, doi: 10.1002/wrcr.20192.

[5] T. Sarkar, A. Karunakalage, S. Kannaujiya, and C. Chaganti, "Quantification of groundwater storage variation in Himalayan & peninsular river basins correlating with land deformation effects observed at different Indian cities," *Contrib. Geophys. Geodesy*, vol. 52, no. 1, pp. 1–56, Apr. 2022, doi: 10.31577/CONGEO.2022.52.1.1.

[6] A. Tripathi, A. R. Reshi, M. Moniruzzaman, K. R. Rahaman, R. K. Tiwari, and K. Malik, "Interoperability of C-band Sentinel-1 SAR and GRACE satellite sensors on PSInSAR-based urban surface subsidence mapping of varanasi, India," *IEEE Sensors J.*, vol. 22, no. 21, pp. 21071–21081, Nov. 2022, doi: 10.1109/JSEN.2022.3208117.

[7] A. P. Saji et al., "Surface deformation and influence of hydrological mass over Himalaya and north India revealed from a decade of continuous GPS and GRACE observations," *J. Geophys. Res., Earth Surf.*, vol. 125, no. 1, Jan. 2020, Art. no. e2018JF004943, doi: 10.1029/2018JF004943.

[8] B. F. Thomas and J. S. Famiglietti, "Identifying climate-induced groundwater depletion in GRACE observations," *Sci. Rep.*, vol. 9, no. 1, Mar. 2019, Art. no. 4124, doi: 10.1038/s41598-019-40155-y.

[9] M. H. Saffi and L. Vijselaar. (2007). *Groundwater Resorces at Risk in Afghanistan*. [Online]. Available: http://www.dacaar.org

[10] G. L. Macpherson, W. C. Johnson, and H. Liu, "Viability of karezes (ancient water supply systems in Afghanistan) in a changing world," *Appl. Water Sci.*, vol. 7, no. 4, pp. 1689–1710, Jul. 2017, doi: 10.1007/s13201-015-0336-5.

[11] T. J. Mack, M. P. Chornack, and I. M. Verstraeten, "Sustainability of water supply at military installations, Kabul Basin, Afghanistan," in *Sustainable Cities and Military Installations* (Northern Atlantic Treaty Organization Science for Peace and Security Series C: Environmental Security), I. Linkov, Ed. U.S. Geological Survey Afghanistan Project, 2014, doi: 10.1007/978-94-007-7161-1_11.

[12] J. F. Shroder, N. Eqrar, H. Waizy, H. Ahmadi, and B. J. Weihs, "Review of the geology of Afghanistan and its water resources," *Int. Geol. Rev.*, vol. 64, no. 7, pp. 1009–1031, Apr. 2022, doi: 10.1080/00206814.2021.1904297.

[13] D. Banks and O. Soldal, "Towards a policy for sustainable use of groundwater by non-governmental organisations in Afghanistan," *Hydrogeol. J.*, vol. 10, no. 3, pp. 377–392, Jun. 2002, doi: 10.1007/s10040-002-0203-y.

[14] A. Zaryab, H. R. Nassery, and F. Alijani, "The effects of urbanization on the groundwater system of the Kabul shallow aquifers, Afghanistan," *Hydrogeol. J.*, vol. 30, no. 2, pp. 429–443, Mar. 2022, doi: 10.1007/s10040-021-02445-6.

[15] A. Muhammad, S. K. Jha, and P. F. Rasmussen, "Drought characterization for a snow-dominated region of Afghanistan," *J. Hydrol. Eng.*, vol. 22, no. 8, Dec. 2017, Art. no. 05017014, doi: 10.1061/(asce)he.1943-5584.0001543.

[16] M. N. Sediqi et al., "Spatio-temporal pattern in the changes in availability and sustainability of water resources in Afghanistan," *Sustainability*, vol. 11, no. 20, p. 5836, Oct. 2019, doi: 10.3390/su11205836.

[17] E. Custodio, "Aquifer overexploitation: What does it mean?" *Hydrogeol. J.*, vol. 10, no. 2, pp. 254–277, Apr. 2002, doi: 10.1007/s10040-002-0188-6.

[18] J. F. Poland and G. H. Davis, "Land subsidence due to withdrawal of fluids," in *Reviews in Engineering Geology*, vol. 2, D. J. Varnes and G. Kiersch, Eds. Geological Society of America, 1969, pp. 187–269, doi: 10.1130/REG2-p187.

[19] K. Terzaghi, "Principles of soil mechanics: I-phenomena of cohesion of clays," *Eng. News Rec.*, vol. 95, no. 19, pp. 742–746, 1925.

[20] Z. Du, L. Ge, A. H.-M. Ng, and X. Li, "Time series interferometry integrated with groundwater depletion measurement from grace," in *Proc. IEEE Int. Geosci. Remote Sens. Symp. (IGARSS)*. Piscataway, NJ, USA: Institute of Electrical and Electronics Engineers, Jul. 2016, pp. 1166–1169, doi: 10.1109/IGARSS.2016.7729295.

[21] G. Meldebekova, C. Yu, Z. Li, and C. Song, "Quantifying ground subsidence associated with aquifer overexploitation using space-borne radar interferometry in Kabul, Afghanistan," *Remote Sens.*, vol. 12, no. 15, p. 2461, Jul. 2020, doi: 10.3390/RS12152461.

[22] H. Save, S. Bettadpur, and B. D. Tapley, "High-resolution CSR GRACE RL05 mascons," *J. Geophys. Res., Solid Earth*, vol. 121, no. 10, pp. 7547–7569, Oct. 2016, doi: 10.1002/2016JB013007.

[23] H. Save, B. Tapley, and S. Bettadpur, "GRACE RL06 reprocessing and results from CSR," *Geophys. Res. Abstr.*, vol. 20, pp. 2018–10697, Apr. 2018.

[24] B. R. Scanlon et al., "Global evaluation of new GRACE mascon products for hydrologic applications," *Water Resour. Res.*, vol. 52, no. 12, pp. 9412–9429, Dec. 2016, doi: 10.1002/2016WR019494.

[25] J. R. Jensen, *Remote Sensing of the Environment: An Earth Resource Perspective*, 2nd ed. Pearson, 2007.

[26] D. Haldar, A. Das, M. Yadav, R. S. Hooda, S. Mohan, and M. Chakraborty, "Analysis of temporal polarization phase difference for major crops in India," *Prog. Electromagn. Res. B*, vol. 57., pp. 299–309, 2014.

[27] C. S. Reddy and K. R. L. Saranya, "Earth observation data for assessment of nationwide land cover and long-term deforestation in Afghanistan," *Global Planet. Change*, vol. 155, pp. 155–164, Aug. 2017, doi: 10.1016/j.gloplacha.2017.07.005.

[28] I. Qutbudin et al., "Seasonal drought pattern changes due to climate variability: Case study in Afghanistan," *Water*, vol. 11, no. 5, p. 1096, May 2019, doi: 10.3390/w11051096.

[29] V. Aich et al., "Climate change in Afghanistan deduced from reanalysis and coordinated regional climate downscaling experiment (CORDEX)—South Asia simulations," *Climate*, vol. 5, no. 2, p. 38, May 2017, doi: 10.3390/cli5020038.

[30] A. S. Qureshi, "Water resources management in Afghanistan: The issues and options," Int. Water Manag. Inst., Pakistan Country Ser. 14, Work. Paper 49, Jun. 2002.

[31] A. Karunakalage et al., "The appraisal of groundwater storage dwindling effect, by applying high resolution downscaling GRACE data in and around Mehsana district, Gujarat, India," *Groundwater Sustain. Develop.*, vol. 13, May 2021, Art. no. 100559, doi: 10.1016/j.gsd.2021.100559.

[32] World Bank. (2018). *Strengthening Hydromet and Early Warning Services in Afghanistan: A Road Map*. [Online]. Available: http://www.worldbank.org

[33] J. F. Shroder. (2014). *Natural Resources in Afghanistan Geographic and Geologic Perspectives on Centuries of Conflict*. [Online]. Available: http://elsevier.com/locate/permissions

[34] C. A. Ruleman, A. J. Crone, M. N. Machette, K. M. Haller, and K. S. Rukstales, "Map and database of probable and possible Quaternary faults in Afghanistan," U.S. Geol. Surv. Open-File Rep. 2007-1103, 2007, p. 39.

[35] D. Banks, "A hydrogeological atlas of Faryab Province, northern Afghanistan," NORPLAN, Faryab Province, Afghanistan, Tech. Rep., Dec. 2014, doi: 10.13140/RG.2.1.1528.9444.

[36] J. W. Whitney, "Geology, water, and wind in the lower Helmand Basin, southern Afghanistan," U.S. Geol. Surv. Sci. Invest. Rep. 2006-5182, 2006, p. 40. [Online]. Available: http://www.usgs.gov/

[37] L. Sinfield and J. Shroder, "Ground-water geology of Afghanistan," in *Transboundary Water Resources in Afghanistan*. Amsterdam, The Netherlands: Elsevier, 2016, pp. 41–90, doi: 10.1016/b978-0-12-801886-6.00003-3.

[38] G. Houben and T. Tunnermeier, "Hydrogeology of the Kabul Basin, Part I: Geology, aquifer characteristics, climate and hydrology," Federal Inst. Geosci. Natural Resour. (BGR), Hanover, Germany, BGR Rec. 10277/05, 2005, pp. 1–52.

[39] M. C. Neves, L. M. Nunes, and J. P. Monteiro, "Evaluation of GRACE data for water resource management in Iberia: A case study of groundwater storage monitoring in the Algarve region," *J. Hydrol., Regional Stud.*, vol. 32, Dec. 2020, Art. no. 100734, doi: 10.1016/j.ejrh.2020.100734.

[40] S. S. Cooley, F. W. Landerer, V. Humphrey, J. T. Reager, and M. M. Srinivasan, "GRACE L-3 product user handbook GRACE D-103133," NASA Jet Propuls. Lab. Pasadena, CA, USA, Tech. Rep. GRACE D-103133, 2020.

[41] D. P. Thoma et al., "Comparison of four models to determine surface soil moisture from C-band radar imagery in a sparsely vegetated semiarid landscape," *Water Resour. Res.*, vol. 42, no. 1, Jan. 2006, doi: 10.1029/2004WR003905.

[42] H. Beaudoing and M. Rodell, "GLDAS Noah Land Surface Model L4 monthly 0.25 × 0.25 degree V2.1, Greenbelt, Maryland, USA, Goddard Earth Sciences Data and Information Services Center (GES DISC)," NASA/GSFC/HSL, 2020. Accessed: Feb. 5, 2022, doi: 10.5067/SXAVCZFAQLNO.

[43] C. S. Chanu, H. Munagapati, V. M. Tiwari, A. Kumar, and L. Elango, "Use of GRACE time-series data for estimating groundwater storage at small scale," *J. Earth Syst. Sci.*, vol. 129, no. 1, Dec. 2020, Art. no. 215, doi: 10.1007/s12040-020-01465-2.

[44] Y. Cao, Z. Nan, and X. Hu, "Estimating groundwater storage changes in the Heihe river basin using grace," in *Proc. IEEE Int. Geosci. Remote Sens. Symp.*, Jul. 2012, pp. 798–801, doi: 10.1109/IGARSS.2012.6351441.

[45] *Standardized Precipitation Index User Guide*, WMO, Geneva, Switzerland, 2012. [Online]. Available: http://www.wmo.int/pages/themes/%20acronyms/index_en.html

[46] C. Funk et al., "The climate hazards infrared precipitation with stations—A new environmental record for monitoring extremes," *Sci. Data*, vol. 2, no. 1, Dec. 2015, Art. no. 150066, doi: 10.1038/sdata.2015.66.

[47] T. B. Mckee, N. J. Doesken, and J. Kleist, "The relationship of drought frequency and duration to time scales," in *Proc. 8th Conf. Appl. Climatol.*, 1993, pp. 17–22.

[48] B. R. Scanlon et al., "Global models underestimate large decadal declining and rising water storage trends relative to GRACE satellite data," *Proc. Nat. Acad. Sci. USA*, vol. 115, no. 6, pp. E1080–E1089, Feb. 2018, doi: 10.1073/pnas.1704665115.

[49] M. Khorasani, M. Ehteshami, H. Ghadimi, and M. Salari, "Simulation and analysis of temporal changes of groundwater depth using time series modeling," *Model. Earth Syst. Environ.*, vol. 2, no. 2, Jun. 2016, Art. no. 90, doi: 10.1007/s40808-016-0164-0.

[50] J. Warren and R. O. Gilbert, "Statistical methods for environmental pollution monitoring," *Technometrics*, vol. 30, no. 3, p. 348, Dec. 1988, doi: 10.2307/1270090.

[51] P. Khambhammettu, "Annual groundwater monitoring report, Appendix D Mann-Kendall analysis for the fort ord site," HydroGeoLog., Inc., Former Fort Ord, CA, USA, OU-1 2004 Annu. Groundwater Monit. Rep., 2005, pp. 1-7.

[52] P. K. Sen, "Estimates of the regression coefficient based on Kendall's tau," *J. Amer. Stat. Assoc.*, vol. 63, no. 324, pp. 1379–1389, Dec. 1968.

[53] Y. Guo et al., "Evaluation of groundwater storage depletion using GRACE/GRACE follow-on data with land surface models and its driving factors in Haihe River Basin, China," *Sustainability*, vol. 14, no. 3, p. 1108, Jan. 2022, doi: 10.3390/su14031108.

[54] J. Xanke and T. Liesch, "Quantification and possible causes of declining groundwater resources in the euro-mediterranean region from 2003 to 2020," *Hydrogeol. J.*, vol. 30, no. 2, pp. 379–400, Mar. 2022, doi: 10.1007/s10040-021-02448-3.

[55] T. Strozzi, U. Wegmüller, L. Tosi, G. Bitelli, and V. Spreckels, "Land subsidence monitoring with differential SAR interferometry," *Photogramm. Eng. Remote Sens.*, vol. 67, no. 11, pp. 1261–1270, 2001.

[56] O. Mora, R. Arbiol, and V. Palà, "ICC's project for DInSAR terrain subsidence monitoring of the Catalonian territory," in *Proc. IEEE Int. Geosci. Remote Sens. Symp.* IEEE, 2007.
[57] F. Casu, A. Manconi, A. Pepe, and R. Lanari, "Deformation time-series generation in areas characterized by large displacement dynamics: The SAR amplitude pixel-offset SBAS technique," *IEEE Trans. Geosci. Remote Sens.*, vol. 49, no. 7, pp. 2752–2763, Jul. 2011, doi: 10.1109/TGRS.2010.2104325.
[58] R. Hanssen, *Radar Interferometry Data Interpretation and Error Analysis*, vol. 2. Dordrecht, The Netherlands: Springer, 2001, doi: 10.1007/0-306-47633-9.
[59] R. Tomás et al., "Mapping ground subsidence induced by aquifer overexploitation using advanced Differential SAR Interferometry: Vega Media of the Segura River (SE Spain) case study," *Remote Sens. Environ.*, vol. 98, nos. 2–3, pp. 269–283, Oct. 2005, doi: 10.1016/j.rse.2005.08.003.
[60] X. Zhou, W. Zhong, D. Tang, and H. Han, "Application of D-InSAR technology in monitoring land-surface subsidence after an earthquake," in *Proc. 7th Int. Conf. Hydraulic Civil Eng.; Smart Water Conservancy Intell. Disaster Reduction Forum (ICHCE; SWIDR)*. Piscataway, NJ, USA: Institute of Electrical and Electronics Engineers, Nov. 2021, pp. 990–995, doi: 10.1109/ICHCESWIDR54323.2021.9656385.
[61] X. Zhou, N.-B. Chang, and S. Li, "Applications of SAR interferometry in Earth and environmental science research," *Sensors*, vol. 9, no. 3, pp. 1876–1912, Mar. 2009, doi: 10.3390/s90301876.
[62] I. Baran, M. P. Stewart, B. M. Kampes, Z. Perski, and P. Lilly, "A modification to the Goldstein radar interferogram filter," *IEEE Trans. Geosci. Remote Sens.*, vol. 41, no. 9, pp. 2114–2118, Sep. 2003, doi: 10.1109/TGRS.2003.817212.
[63] X. L. Ding, G. X. Liu, Z. W. Li, Z. L. Li, and Y. Q. Chen, "Ground subsidence monitoring in Hong Kong with satellite SAR interferometry," *Photogramm. Eng. Remote Sens.*, vol. 70, no. 10, pp. 1151–1156, Oct. 2004.
[64] R. S. Chatterjee et al., "Subsidence of Kolkata (Calcutta) city, India during the 1990s as observed from space by differential synthetic aperture radar interferometry (D-InSAR) technique," *Remote Sens. Environ.*, vol. 102, nos. 1–2, pp. 176–185, May 2006, doi: 10.1016/j.rse.2006.02.006.
[65] D. H. O. T. Minh et al., "Quantifying horizontal and vertical movements in Ho Chi Minh City by Sentinel-1 radar interferometry," *Preprints*, 2020, doi: 10.20944/preprints202012.0382.v1.
[66] M. Manzo et al., "Surface deformation analysis in the Ischia Island (Italy) based on spaceborne radar interferometry," *J. Volcanology Geothermal Res.*, vol. 151, no. 4, pp. 399–416, Mar. 2006, doi: 10.1016/j.jvolgeores.2005.09.010.
[67] Z. Yang et al., "An alternative method for estimating 3-D large displacements of mining areas from a single SAR amplitude pair using offset tracking," *IEEE Trans. Geosci. Remote Sens.*, vol. 56, no. 7, pp. 3645–3656, Jul. 2018, doi: 10.1109/TGRS.2018.2803285.
[68] *Afghanistan Resource Corridor Development: Water Strategy Final Kabul River Basin Report*, World Bank, Kabul, Afghanistan, Jun. 2012.
[69] M. R. Taher, M. P. Chornack, and T. J. Mack, "Groundwater levels in the Kabul Basin, Afghanistan, 2004–2013," U.S. Geol. Surv. Open-File Rep. 2013-1296, 2014, p. 51, doi: 10.3133/ofr20131296.

Mohammad Taqi Daqiq received the bachelor's degree in geology from the University of Bamyan, Bamyan, Afghanistan, in 2016, and the master's degree in applied geology from the Indian Institute of Technology Roorkee, Roorkee, India, in 2022, where he is currently pursuing the Ph.D. degree in Earth sciences.

His research focuses on application of remote sensing and geophysics for subsurface fluid exploration, particularly groundwater, and geothermal resources. He also specializes in synthetic aperture radar (SAR) and Gravity Recovery and Climate Experiment (GRACE) data applications.

Mr. Daqiq, beyond his academic pursuits, is an active member of prominent organizations, such as the American Geophysical Union (AGU), Society of Exploration Geophysicists (SEG), Society of Petroleum Engineers (SPE), the Society of Petrophysicists and Well Log Analysts (SPWLA), and the London Petrophysical Society (LPS). His scholarly dedication is underscored by his sponsorship from the Indian Council for Cultural Relations (ICCR) and recognition through the Berkner Travel Fellowship awarded by AGU23.

Ravi Sharma (Member, IEEE) received the master's degree in applied geophysics from the University of Roorkee, Roorkee, India, in 1999, and the M.S. and Ph.D. degrees in petroleum engineering from the Colorado School of Mines, Golden, CO, USA, in 2015.

He has extensive work experience in various roles in the hydrocarbon energy industry. His research interests include experimental and modeling methods in rock physics and petrophysics for storage, flow, and the associated elastic and geomechanical property determination, integrated reservoir (convention and unconventional) characterization, machine learning (ML), artificial intelligent (AI) applications in geosciences, and petroleum engineering.

Dr. Sharma is an active member of the American Geophysical Union (AGU), IEEE, Society of Exploration Geophysicists (SEG), Society of Petroleum Engineers (SPE), American Association of Petroleum Geologists (AAPG), Society of Petroleum Geophysicists (SPG), and Society of Petrophysicists and Well Log Analysts (SPWLA), an Associate Editor of the *Journal of Applied Geophysics* and *Geohorizons*, and a Guest Editor of *Frontiers in Earth Science*.

Anuradha Karunakalage received the Bachelor of Science degree with major in geology from the University of Peradeniya, Sri Lanka, in 2017, the first master's degree in remote sensing and geographic information system (GIS) from the Indian Institute of Remote Sensing (IIRS), ISRO, Dehradun, India, and the second master's degree in applied geology from the Department of Earth Sciences (ESD), Indian Institute of Technology (IIT) Roorkee, Roorkee, India, where she is currently pursuing the Ph.D. degree.

She is an Alumna and bronze medallist of the UN-affiliated Centre for Space Science and Technology Education in Asia and the Pacific (CSSTEAP), and the Indian Institute of Remote Sensing, ISRO, where she earned her first post-graduation in Remote Sensing and GIS in 2020. She also served as a consultant at the International Water Management Institute headquarter, Colombo, Sri Lanka. Her research interests encompass hydrogeology, land subsidence, applications of GRACE data, synthetic aperture radar (SAR) applications, the use of GNSS data for natural hazard prediction, and climate change.

Suresh Kannaujiya received the M.Tech. degree from the Indian Institute of Technology (IIT) Roorkee, Roorkee, India, in 2011, and the Ph.D. degree from IIT ISM Dhanbad, Dhanbad, India, in 2022, both in applied geophysics.

He has been working as a Scientist with the Geosciences Department, Indian Institute of Remote Sensing, ISRO, Dehradun, India, for the last ten years. He is working on geodynamics, groundwater, natural hazards and geophysical applications. His primary interests include modeling global navigation satellite system (GNSS) data for total electron content/strain/crustal deformation, analyzing the consequence of land deformation due to groundwater exploitation, and active fault mapping through the geophysical survey.